quaternary

MDPI

Article

Hydroclimatic Changes Revealed by Multiple Proxies Since the Last Glacial Maximum from the Core Monsoon Zone of India

Mohammad Firoze Quamar [1,2,*], Jyotsna Dubey [1,3], Pooja Tiwari [1], Prasanta Kumar Das [1], Biswajeet Thakur [1,2], Mohammad Javed [1,3], Nagendra Prasad [1,2], M. E. T. Maneesha [1,2] and Satish J. Sangode [4]

[1] Birbal Sahni Institute of Palaeosciences (BSIP), Lucknow 226007, India
[2] Academy of Scientific and Innovative Research (AcSIR), Ghaziabad 201002, India
[3] Department of Geology, University of Lucknow, Lucknow 226007, India
[4] Department of Geology, Savitribai Phule Pune University (S.P.P.U.), Pune 411007, India
* Correspondence: mohdfiroze_quamar@bsip.res.in

Abstract: We present multiproxy records from a 2.25-m-long lake sediment profile from central India, which suggested that between ~22,200 and 18,658 cal yr BP, the Indian Summer Monsoon (ISM) was weak, supporting open vegetation in a cool and dry climate, which is globally correlated with the Last Glacial Maximum (LGM). The grain size data of this phase suggest low-energy conditions, indicating a weak ISM. Environmental magnetic concentration-dependent parameters also confirm this weakened ISM. Between ~18,658 and 7340 cal yr BP, the ISM underwent a notable increase, and open mixed tropical deciduous forests replaced the existing vegetation under a warm and moderately humid climate. Environmental magnetic parameters and the grain size data signal a shift toward higher energy levels, in harmony with the warm and moderately humid climate during this time span. Between ~7340 and 1960 cal yr BP, the ISM intensity further increased, which supported open mixed tropical deciduous forests with a rise in prominent tree species under a warm and a relatively more humid climate, correlated with the global Holocene Climatic Optimum (HCO). The trends in environmental magnetic parameters and grain size data mirror this phase of climatic amelioration. From ~1961 cal yr BP to the present, the ISM has intensified, giving rise to dense mixed tropical deciduous forests under a warm and relatively more humid climate. Environmental magnetic parameters and the grain size data are in tandem with the palynogical findings from this phase of the ISM variability.

Keywords: multiple proxies; palynology; grain size; environmental magnetism; ISM; Inter-Tropical Convergence Zone (ITCZ); summer insolation and SST; Last Glacial Maximum (LGM)

Citation: Quamar, M.F.; Dubey, J.; Tiwari, P.; Das, P.K.; Thakur, B.; Javed, M.; Prasad, N.; Maneesha, M.E.T.; Sangode, S.J. Hydroclimatic Changes Revealed by Multiple Proxies Since the Last Glacial Maximum from the Core Monsoon Zone of India. *Quaternary* **2024**, *7*, 52. https://doi.org/10.3390/quat7040052

Academic Editor: Anna Maria Mercuri

Received: 27 May 2024
Revised: 19 August 2024
Accepted: 10 September 2024
Published: 21 November 2024

1. Introduction

The Indian summer monsoon (ISM) (also known as the Southwest Monsoon: SWM, the Southwest Summer Monsoon: SWSM, the South Asian Summer Monsoon: SASM, or simply, the monsoon and Indian Summer Monsoon rainfall: ISMR) is a major component of the Asian Monsoon System—a large-scale phenomenon affecting the ocean, land, and atmosphere [1–7]. The ISM is the backbone of the socio-economic well-being of the people in Africa and Southeast Asia, including India [8]. Around 80–90% of the total rainfall during the months of June to September (JJAS) is caused by the ISM, which is a prerequisite for agricultural productivity (Kharif crops), the economy and societal benefits in the Indian subcontinent [9–13]. El Niño, La Niña, the Indian Ocean Dipole and Walker circulation in the equatorial Pacific influence the ISM [14,15]. The movement of the Inter-Tropical Convergence Zone (ITCZ) over the equatorial region, however, is regarded as the cause of monsoons [16]. The seasonal northward movement of the ITCZ due to the warming of the Asian continents during the summer initiates the summer rains associated with the Southwest Monsoon (SWM) [17]. The intensity of ISM precipitation varies in different Indian basins owing to the variations in latitude, altitude and distance from the

sea [18]. These variations in the ISMR cause extreme floods, landslides (in the Himalaya) or droughts, which affect >60% of the world's population over much of South and East Asia [5,10] and are closely associated with the prosperity of and/or decline in ancient human civilizations [19–25]. The occurrences of such events from the Indian subcontinent allow and/or force us to adopt the measures of adaptation and mitigation [26,27]. Further, droughts and floods over India and other parts of South Asia potentially are impacts of ISM variations, directly affecting the agricultural output, economic development and societal well-being of this densely populated region [8,10–12,22].

Saraswat et al. [28] briefly summarized the evolution of the monsoon system, taking into account previous studies using both terrestrial and marine records generated from the Indian subcontinent and the adjoining seas. Srivastava et al. [29] have both qualitatively and quantitatively reconstructed the monsoonal discrepancies during the last ~44 ka using the coexistence approach (CA) and concluded that the extended period of rainfall during the Late Pleistocene was because of the monsoonal, post-monsoonal and pre-monsoonal rainfall, which supported the growth and sustenance of wet evergreen elements in the Western Ghats. Moreover, our knowledge and understanding of the variability in ISMR is important both to understand present climatic conditions and to make predictions of future climactic conditions [30–32]. Therefore, keeping in mind the significance of the ISMR for the socio-economic well-being of the people in Southeast Asia and India, the present study was carried out on a 2.25-m-long sediment profile from a lacustrine area, named as Anandpur Nursery Lake (ANL), of the Baikunthpur Forest Range of the Koriya District (Chhattisgarh), central India, which comes under the core monsoon zone (CMZ) of India, using pollen, grain size and magnetic susceptibility/environmental magnetism data.

Palaeoarchives, such as marine sediments [33–36], lacustrine sediments [37–41], speleothems [42–44] and tree rings [45,46], have been widely used to reconstruct the ISMR variability with varying temporal resolution. Lake sediments, compared to marine sediments, provide direct evidence of past events on a local or regional scale, with a relatively high temporal resolution [47,48]. The main objective of the present study was to reconstruct the ISMR variability since the Last Glacial Maximum (LGM) using the multi-proxy approach (pollen, grain size and environmental magnetism) on the lacustrine sediments in the Koriya District (Chhattisgarh State, central India), falling under the CMZ of India. We also interrelated the results with published pollen data from palaeovegetation and palaeoclimatic reconstructions in the central Indian CMZ [49].

2. Regional Setting

2.1. Study Area

Anandpur Nursery Lake (ANL) is located about 20 km north of the Baikunthpur Township (82°32′58.66″ E: 23°14′59.98″ N; 529 m a.s.l.) of the Koriya District in Chhattisgarh State (Figure 1).The area adjacent to the site of investigation is marked by highlands of low relief with gorges. Hilly soils and sandy soil are chiefly found in the area. Rice, maize, wheat and pulses are cultivated in the area by the local farmers and tribes.

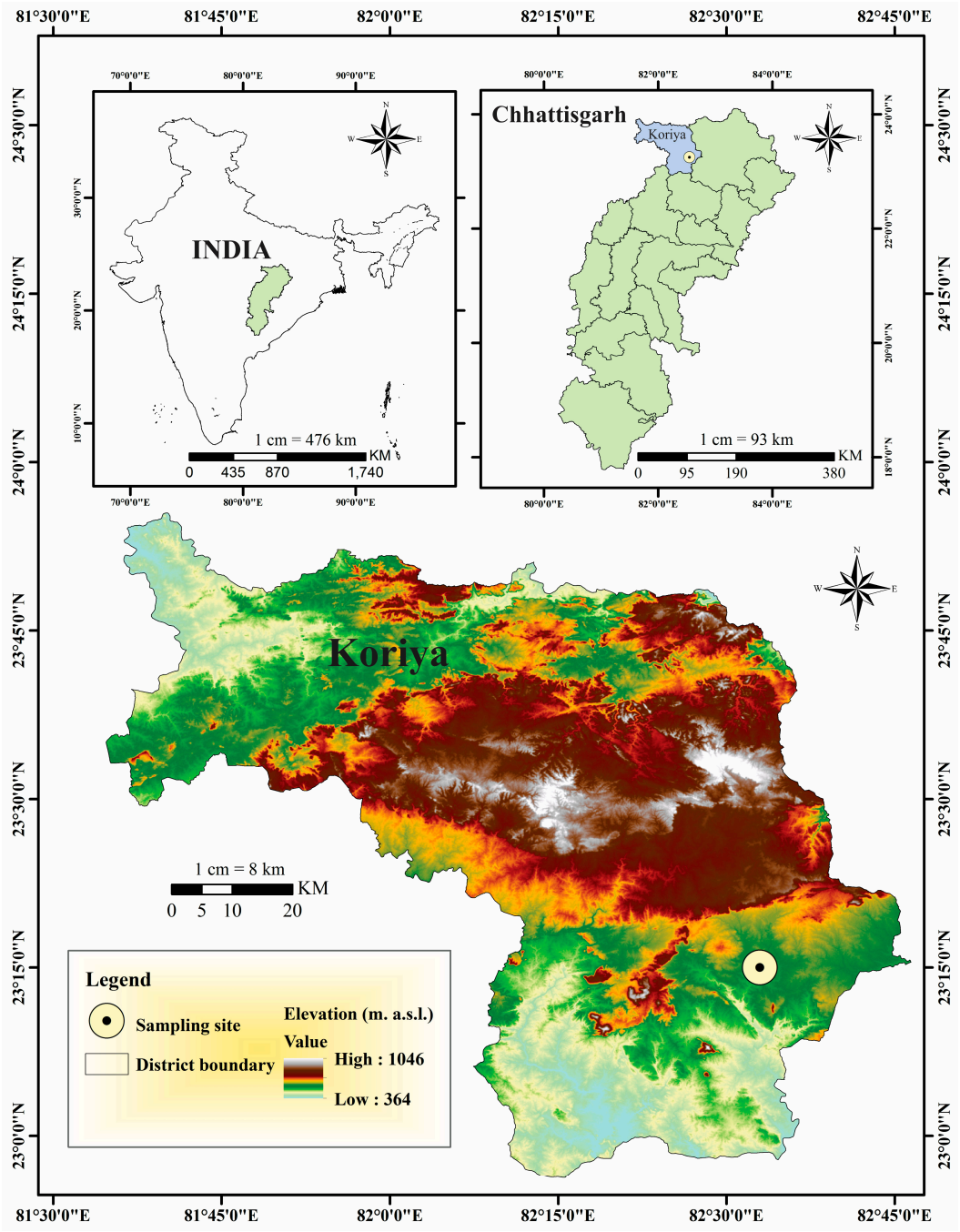

Figure 1. Geographical map of India showing Chhattisgarh State (**upper-left panel**), geographical map of Chhattisgarh State, central India showing the Koriya District (**upper-right panel**), and Shuttle Radar Topographic Mission (SRTM) and digital elevation model (DEM) showing the sampling site in the Koriya District (**lower panel**). Figure 1 was created using ArcGIS 10.3.

2.2. Climate

A tropical savannah-type climate (Aw) and Mesothermal-Gangetic Plain-type climate (Cwg) are found in the study area [50,51]. The nearest Climate Research Unit (CRU) Time-series (TS) (version 4.06) data are represented in Figure 2, with 0.5 × 0.5 gridded climate data points for 1901–2021 showing the mean monthly precipitation and temperature in the lacustrine deposit of the Koriya District [52]. The mean annual temperature (MAT) is 24.449 (24.45) °C, and the mean annual precipitation (MAP) is 1290.72 (~1291) mm in the study area in the Koriya District (Figure 2).

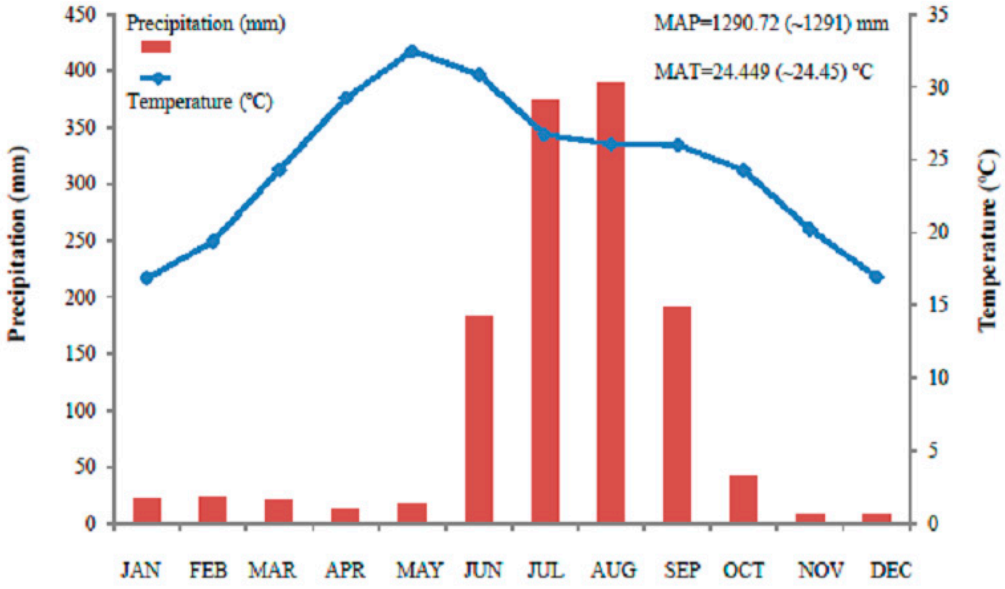

Figure 2. Nearest CRU TS (version 4.06) data with 0.5 × 0.5 gridded climate data points for 1901–2021 showing mean monthly precipitation and temperature around the ANL of the Koriya District, Chhattisgarh State, central India. These data are 121-year climate averages for the period of 1901–2021; MAP = mean annual precipitation; MAT = mean annual temperature.

2.3. Vegetation

Both moist and dry tropical deciduous forests dominated by teak (*Tectona grandis*) and sal (*Shorea robusta*) occupy the landscape in the study area in the region [51,53]. The commonassociates of the forests are shown in Table 1.

Table 1. Common associates of the forests in the study area.

Name of Taxa	Habits	Name of Families
Madhucaindica J. F. Gmelin	Tree	Sapotaceae
Terminaliachebula Retz	Tree	Combretaceae
T. bellerica (Gaertn.) Roxb.	Tree	Combretaceae
T. arjuna (Roxb. ex DC.) Wight et Arn.	Tree	Combretaceae
T. tomentosa Wight et Arn.	Tree	Combretaceae
Azadirachta indica A. Juss.	Tree	Meliaceae
Diospyros melanoxylon Roxb.	Tree	Ebenaceae
Schleichera oleosa (Lour.) Oken.	Tree	Sapindaceae
Syzygium cumini (L.) Skeels	Tree	Myrtaceae
Buchanania lanzan Spreng.	Tree	Anacardiaceae
Acacia catechu (L. f.) Willd.	Tree	Mimosaceae
Dalbergia sissoo Roxb.	Tree	Fabaceae
Boswellia serrata Roxb. ex.- Colebr	Tree	Burseraceae
Holoptelea integrifolia Planch.	Tree	Ulmaceae
Gmelina arborea Roxb.	Tree	Lamiaceae
Aeglemarmelos (L.) Correa	Tree	Rutaceae
Emblica officinalis Gaertn.	Tree	Euphorbiaceae
Anthocephaleous cadamba (Roxb.) Miq.	Tree	Rubiaceae

Table 1. *Cont.*

Name of Taxa	Habits	Name of Families
Lagerstroemi aparviflora Roxb.	Tree	Lythraceae
Mitragyna parvifolia (Roxb.) Korth.	Tree	Rubiaceae
Adina cordifolia (Roxb.) Hook. f. ex.- Bedd.	Tree	Rubiaceae
Eucalyptus sp. L'Hér.	Tree	Myrtaceae
Butea monosperma (Lam.) Taub.	Tree	Fabaceae
Ficus benghalensis L.	Tree	Moraceae
Semecarpus anacardium L.f.	Tree	Anacardiaceae
Ziziphus mauritiana Lam.	Shrub	Rhamnaceae
Strobilanthes sp.	Shrub	Acanthaceae
Acacia spp.	Shrub	Mimosaceae
Holarrhena antidysenterica (L.) Wall.	Shrub	Apocynaceae
Ricinus communis L.	Shrub	Euphorbiaceae
Grasses (Members of Poaceae)	Terrestrial herb	Poaceae
Ageratum conyzoides L.	Terrestrial herb	Asteraceae
Sida rhombifolia Roxb. ex Fleming	Terrestrial herb	Malvaceae
Hyptis suaveolens (L.) Poit	Terrestrial herb	Lamiaceae
Blumea spp.	Terrestrial herb	Asteraceae
Leucas aspera (Willd.) Link.	Terrestrial herb	Lamiaceae
Chenopodium album L.	Terrestrial herb	Amaranthaceae
Amaranthus spinosa L.	Terrestrial herb	Amaranthaceae
Achyranthes aspera L.	Terrestrial herb	Amaranthaceae
Xanthium strumarium L.	Terrestrial herb	Asteraceae
Mazus japonicas (Thunb.) Kuntze	Terrestrial herb	Mazaceae
Sonchus spp.	Terrestrial herb	Asteraceae
Oxalis acetocella	Terrestrial herb	Oxalidaceae
Justicia simplex D. Don.	Terrestrial herb	Acanthaceae
Euphorbia hirta L.	Terrestrial herb	Euphorbiaceae
E. thymifolia L.	Terrestrial herb	Euphorbiaceae
Ajuga sp.	Terrestrial herb	Lamiaceae
Commelina benghalensis L.	Terrestrial herb	Commelinaceae
Scirpus sp.	Marshy herb	Cyperaceae
Cyperus rotundifolia L.	Marshy herb	Cyperaceae
Carex sp.	Marshy herb	Cyperaceae
Ammania baccifera L.	Marshy herb	Lythraceae
Rumex sp.	Marshy herb	Polygonaceae
Polygonum plebieum R. Br.	Marshy herb	Polygonaceae
P. serrulatum Lag., *Menthaarvensis* L.	Marshy herb	Polygonaceae
Mentha arvensis L.	Marshy herb	Lamiaceae
Hygrophila auriculata (Schumach.) Heyne.	Marshy herb	Acanthaceae
Pimpinella tomentosa (Dalzell & Gibson) C.B. Clarke	Marshy herb	Apiaceae
Solanum xanthocarpum Schrad et Wendl.	Marshy herb	Solanaceae

Table 1. *Cont.*

Name of Taxa	Habits	Name of Families
Ocimum americanum L.	Marshy herb	Lamiaceae
O. sanctum L.	Marshy herb	Lamiaceae
Typha latifolia L.	Aquatic herb	Typhaceae
Trapa sp.	Aquatic herb	Trapaceae
Nymphoides indica (L.) Kuntze	Aquatic herb	Menyanthaceae
Potamogeton purpurascens Seidi ex J. Presl et C. Presl	Aquatic herb	Potamogetonaceae
Lemna paucicostata Hegelm.	Aquatic herb	Araceae
Dryopteris prolifera (Retz.) C. Chr.	Pteridophytic herb	Dryopteridaceae
Adiantum philippensis L.	Pteridophytic herb	Pteridaceae
Diplazium esculentum (Retz.) Sw.	Pteridophytic herb	Athyriaceae
Selaginella semicordata N. Wall.	Pteridophytic herb	Selaginellaceae
Lycopodium cernuum	Pteridophytic herb	Lycopodiaceae

3. Materials and Methods

3.1. Field Work, Coring, Sampling Method and Lithological Details

A 2.25 m-long-lacustrine sediment profile was collected for the present study from the Baikunthpur Forest Range of the Koriya District (Chhattisgarh), central India. In total, 30 samples were collected for this profile: 15 samples at 5 cm intervals (10 samples from 0 to 50 cm and 5 samples from 200 to 225 cm) and the remaining 15 samples at 10 cm intervals (50–200 cm). Additionally, bulk samples were also taken at larger intervals for radiocarbon dating. Three prominent lithozones can be seen from top to bottom in the profile, based on the variation in sediment texture at different depths. The top-most lithozone is composed of blackish clay soil with rootlets followed by brownish/blackish clay without rootlets. The bottom-most stratum consists of blackish/brownish clayey soil.

3.2. Radiocarbon (^{14}C) Dating and Chronology

Three samples have been radiocarbon-dated (17,210 ± 670 yr BP at 215 cm depth, 2900 ± 130 yr BP at 90 cm depth and 100 ± 90 yr BP at 40 cm depth) using conventional radiocarbon-dating technique at the Birbal Sahni Institute of Palaeosciences (BSIP), Lucknow (India). IntCal 13 calibration curve [54] was used to calibrate these conventional ^{14}C dates in OxCal software version 4.3 [55]. To establish the age–depth relationship, a Poisson process deposition model (Bayesian age-depth modelling [56]) was followed. All of the model's agreement indices and convergence indices were higher than the critical values; thus, all three ^{14}C samples were kept in the model. For details of the dating and chronology, please see Quamar and Bera [49]. Nonetheless, the Bayesian age-depth model of the ANL, constructed using the R package rbacon [57], is shown in Figure 3.

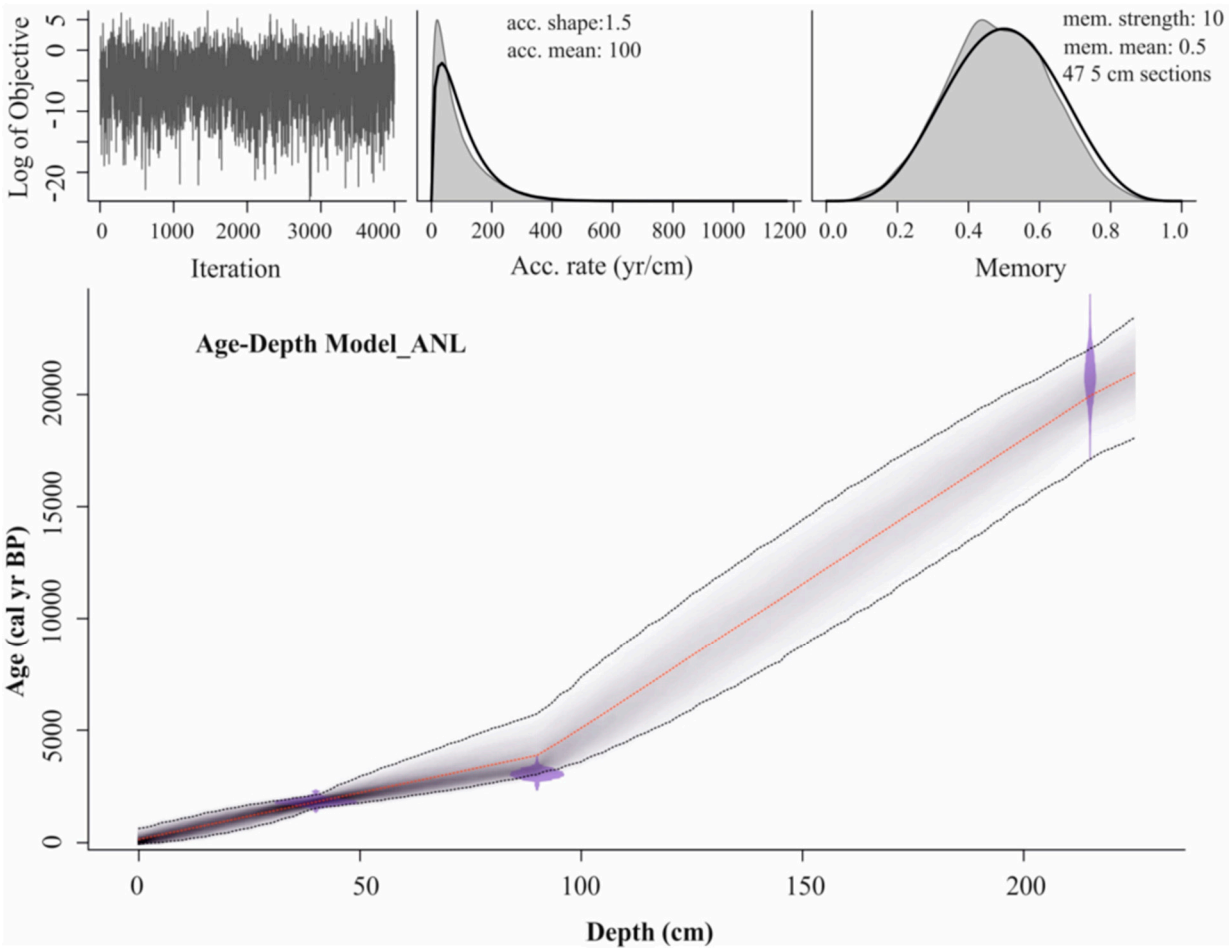

Figure 3. Bayesian age-depth model of the ANL constructed using the R package rbacon [57]). The blue bars indicate the ^{14}C age distribution, whereas the greyscale of the line graph reflects the likelihood and the dotted red line indicates the mean ages. Further details can be had by consulting the paper [49]. (For interpretation of the references to colour in this figure legend, the reader is referred to the web version of this article).

3.3. Pollen Preparation, Microscopic Examination and Pollen Diagram Constructions

Extraction of the palynomorphs (pollen and spores) from the sediment samples is performed following Erdtman's conventional method [58]. Chemical treatments successfully removed humus, silica and cellulose using 10% KOH, 40% HF and an acetolysis mixture consisting of concentrated sulphuric acid (H_2SO_4) and acetic anhydride ($C_4H_6O_3$) in 1:9 ratio, respectively. The samples were finally prepared in 50% glycerine solution for microscopic examination. A few drops of phenol were also added to avoid any microbial contamination.

Pollen and spores were counted under a transmitted light microscope (Olympus BX50, Tokyo, Japan). Pollen and spores were identified using published reference material [39,59–64] and the reference collections held at the BSIP Herbarium. More than 300 terrestrial pollen grains were counted per sample. Pollen percentages were calculated using the total pollen sum (TPS) of terrestrial plants only. Pollen of aquatic plants, marshy taxa, spores of algae and ferns, drifted/transported pollen (transported from higher reaches, i.e., the Himalaya) and fungi were excluded from the TPS; however, their percentages were calculated using the TPS.

3.4. Grain Size (Particle Size)

The sediment samples were initially treated with 10% HCl and 30% H_2O_2 in order to remove the carbonates and organic fractions [65]. Thereafter, to avoid flocculation,

5% solution of sodium hexametaphosphate was added to the samples. The samples were then analysed for grain size using laser particle size analyser (Beckman Coulter LS™ 13 320, Brea, CA, USA) at the Birbal Sahni Institute of Palaeosciences (BSIP), Lucknow, India. The percentages of grain size were determined, such as clay (<2 μm), silt (2–63 μm) and sand fractions (63–2000 μm), following Udden [66] and Wentworth [67]. The grain size was then transferred in Gradistat to obtain the values in phi (∅) scale. Statistics, such as mean, sorting, skewness and kurtosis, were calculated to determine the energy conditions and depositional settings [68].

3.5. Envirnmental Magnetism

Room-temperature rock magnetic analysis was performed following the standard techniques of Walden [69]. Dried and disaggregated sediment samples were gently crushed into powder using an agate mortar and pestle and then packed into standard 10 cm^3 non-magnetic plastic bottles. Low-frequency magnetic susceptibility (χ_{lf}) measurements were carried out with a Bartington susceptibility meter (MS2) coupled with the 2B sensor, which operated at a frequency of 0.465 kHz with a peak field of 200 A/m. In order to see any significant proportion of ultrafine super-paramagnetic grains (SP) of magnetite crystals, frequency variation of χ, expressed in percentage (χ_{FD}%), was measured for the samples at two different frequency values of 0.465 kHz and 4.65 kHz using the MS2B sensor. The anhysteretic remanent magnetization (ARM) was found by exposing the samples to an alternatingly decaying magnetic field with a100 mT peak field anda decay rate of 0.01 mT, in the presence of a direct current (DC) bias field of 0.1 mT using an AGICO alternating field demagnetizer.The ARM intensity was measured using a Minispin fluxgate spinner magnetometer (Molspin, Witney, UK). The susceptibility of ARM (χARM) was calculated by normalizing the ARM with the size of the DC biasing field (i.e., 0.1 mT).

An impulse magnetiser (MODEL IM-10-30; ASC Scientific, Narragansett, RI, USA) was used to impart magnetization to the samples. Progressive forward acquisition of the remanent magnetisation was performed at 0 mT to 1000 mT in six intermediate steps. The remanent magnetization obtained at the 1000 mT pulse field is considered as the saturation isothermal remanent magnetization (SIRM). Progressive backfield demagnetization of the SIRM was performed at 10 mT to 300 mT in six intermediate steps. A JR-6 dual-speed spinner magnetometer (AGICO Ltd., Brno, Czech Republic) was used to measure the remanent magnetization at each acquisition and demagnetization step in the high-speed mode. The S-ratio was computed to measure the relative concentration of soft and hard magnetic minerals in the samples by calculating the ratio of absolute value of IRM at −300 mT over SIRM, i.e., $IRM_{-300mT}/SIRM_{1000mT}$. To obtain absolute concentration of low/hard coercive magnetic minerals, Soft-IRM (calculated as SIRM-|IRM_{-30mT}) and Hard-IRM (calculated as SIRM-IRM_{-300mT}) were derived from the IRM acquisition and demagnetization measurements. The inter-parametric ratios like χARM/SIRM, χARM/χlf and SIRM/χlf, which were indicative of magnetic grain size, were finally calculated [69–78]. Magnetic measurements were performed at the Rock Magnetic Laboratory, Department of Geology, Savitribai Phule Pune University (S.P.P.U.), Pune (Maharashtra), India.

4. Results

4.1. Description of Pollen Diagram

The pollen diagram (Figure 4) has been divided into four distinct pollen zones (ANL-I, ANL-II, ANL-III and ANL-IV), based on the varying frequencies of the prominent arboreal pollen (AP) and non-arboreal pollen (NAP) taxa in order to decipher the sequential vegetation changes and contemporary climatic changes in a chronological order in the region. The pollen zones numbered from the lowest to the highest depths in the Lake sediments profile are described below:

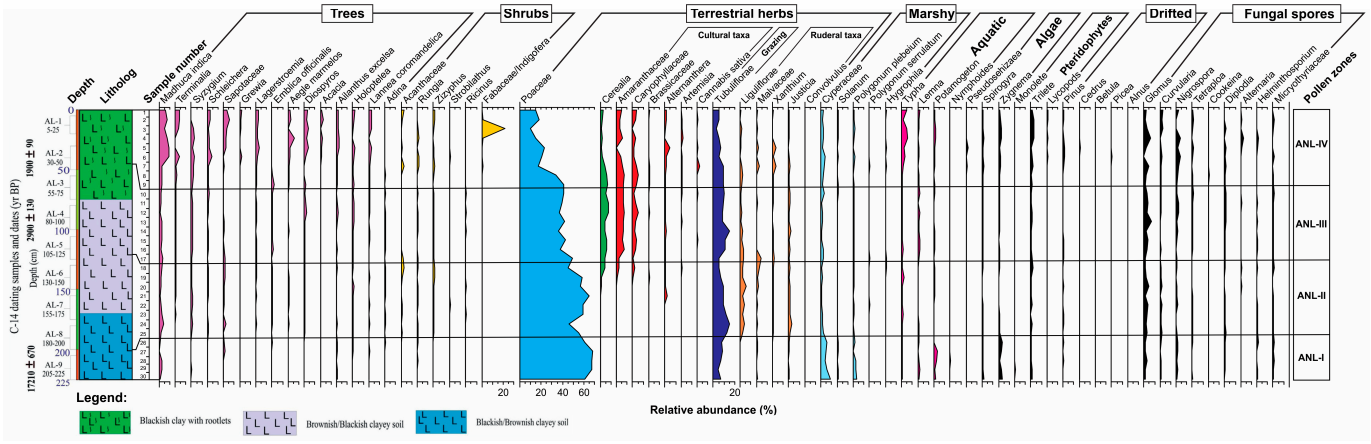

Figure 4. Pollen diagram of tree taxa, shrubs and herbaceous taxa, as well as aquatic taxa, algal remains, marshy taxa, pteridophytic taxa, transported (drifted) taxa and fungal spores from the Anandpur Nursery Lake sediment profile, Koriya District, Chhattisgarh, central India. The pollen zones are designated with the initials 'ANL' after the name of the site of investigation: Anandpur Nursery Lake.

4.1.1. Pollen Zone ANL-I (200–225 cm)

This pollen zone has a single radiocarbon date of 17,210 ± 670 cal yr BP (a 225–200 cm depth) and spans between ~22,200 and 18,658 cal yr BP, suggesting open vegetation. Tree taxa have 3.46% pollen (on average) in the TPS, whereas shrubs have an average value of only 0.43% pollen. Poaceae has 53.31% pollen (on average) in the TPS. Cerealia has <1% pollen, whereas other cultural pollen taxa have <1% pollen in the TPS. Tubuliflorae (Asteroideae: Asteraceae), with an average of 6.53% pollen is followed by other terrestrial herbs, which have only an average of 1.67% pollen in the TPS. Wetland taxa have an average value of 6.67% pollen in pollen rain. Aquatic taxa and algal spores have lower values (2.78% and 2.84%, respectively). Pteridophytic spores and drifted pollen taxa had low values (<1%). Fungal spores are recorded in variable frequencies in this pollen zone.

Thus, open vegetation occupied the landscape in the study area between ~22,200 and 18,658 cal yr BP under a dry climate, probably indicating a reduced level of ISMR. Based on the stray pollen of Cerealia, if considered to be cultivated [79,80], a primitive type of agriculture practice may be assumed in the study area, but wild rice also produces large Cerealia grains [81,82]. Hence, the inception of any primitive agricultural practices was ruled out as this large size criterion may not be applicable to India. Moreover, stray pollen of Amaranthaceae and *Cannabis sativa* has also been recorded, which may indicate land clearance for the purpose of agriculture. But their very small values may not be considered as additional evidence of the possible presence of any sort of primitive agriculture [83]. Freshwater algae, as well as aquatic taxa demonstrate the existence of a lake. The presence of wetland taxa also indicates swampy conditions. Pteridophytic fern spores grew locally in the moist and shady places close to the lake. The scant presence of drifted pollen indicates restricted wind transport from the Himalayas.

4.1.2. Pollen Zone ANL-II (120–200 cm)

This pollen zone with dates ranging between ~18,658 and 7340 cal yr BP shows open mixed tropical deciduous forests. Trees and shrubby taxa have 8.48% and 2.33% pollen values (on average), respectively, in the TPS. Poaceae has a 48.54% pollen value (on average) in the TPS and decreased comparatively. Cerealia (with an average of ~1%) and other cultural plant pollen taxa have <1% pollen in the TPS. Tubuliflorae (with an average of 7.94% pollen) and other terrestrial herbs (with an average of 5.88% pollen) increased comparatively. Wetland taxa have an average of 2.35% pollen. Aquatic taxa, algal remains and pteridophytic fern spores decreased comparatively (with an average of 1.84%, 0.85% and 0.87%, respectively). Drifted pollen taxa had low values (with an

average of 0.29% pollen). Fungal spores are recorded with variable high-to-low values in this pollen zone.

The open vegetation was, thus, succeeded by open mixed tropical deciduous forests between ~18,658 and 7340 cal yr BP under a warm and moderately humid climate, probably indicating increased ISMR. Agricultural practice could not be confirmed during this timeframe, as Cerealia and other cultural pollen taxa do not show much variation. The continuous sediment influx affected lake dimensions, which became comparatively narrow. This is also shown by comparative reduced frequencies of aquatic taxa, as well as algal spores. The swampy conditions, however, increased a bit in response to the increased level of human activities, as well as the increased frequencies of wetland taxa. The meagre presence of transported taxa denotes their transportation from the Himalayas.

4.1.3. Pollen Zone ANL-III (45–200 cm)

This pollen zone with a solitary date of 2900 ± 130 cal yr BP (an 80–100 cm depth) and time range of ~7340 to 1961 cal yr BP again shows the presence of open mixed tropical deciduous forests. Tree taxa increased comparatively with a 15.47% pollen value (on average) in the TPS, whereas the shrubby taxa (with an average of 1.52% pollen), decreased comparatively. Poaceae shows comparatively decreased values of 38.48% pollen (on average) in the TPS. Cerealia and other cultural pollen taxa increased comparatively with values of 6.66% and 13.28% (on average), respectively. Tubuliflorae (with an average of11.78%) had increased values compared to those during the two preceding pollen zones; however, the other terrestrial herbaceous taxa (with an average of 4.07% pollen) have lower values in this pollen zone. Wetland taxa (with an average of 3.43% pollen) have lower values compared to the preceding pollen zones. Aquatic taxa (with an average of 3.21% pollen), algal remains (with an average of1.73%) and pteridophytic spores (<1%) are sparse. Drifted pollen has very low values (<1% pollen). Fungal spores were recorded with high-to-low values in this pollen zone.

The open mixed tropical deciduous forest became relatively denser than that developed earlier during the preceding phase under a warm and relatively more humid climate, owing to a comparatively increased amount of ISMR between ~7340 and 1961 cal yr BP. Agricultural practice and other anthropic activities became more evident during this phase. Furthermore, intensive pastoral activities are indicated by a comparative increase in Tubuliflorae pollen around the forest area and heathland [84]. The lake became comparatively wider in dimension and swampy conditions prevailed. The drifted pollen indicated it was exclusively transported from the Himalayas.

4.1.4. Pollen Zone ANL-IV (0–45 cm)

This pollen zone, datedto 1900 ± 90 cal yr BP (a 5–25 cm depth) and with the time range of ~1961 cal yr BP to the present, reveals the presence of a relatively dense, mixed tropical deciduous forest. Tree and shrubby taxa have average high values of 28.59% pollen and 6.8% pollen, respectively, compared to the preceding pollen zones. Poaceae show comparatively decreased values, with 18.75% pollen (on average) in the TPS. Comparatively, Cerealia and other cultural pollen taxa decreased a bit with average values of 2.09% and 9.25%, respectively. Tubuliflorae (with an average of 5.77% pollen) have lower values as compared to the three preceding pollen zones, whereas the other terrestrial herbaceous taxa (with an average of 3.67%) have increased values compared to the preceding pollen zone. Wetland taxa (marshy taxa) (with an average of 2.50% pollen) increased a bit compared to the two preceding pollen zones. Aquatic taxa (with an average of 5.49% pollen), algal remains (with an average of 3.21%) and pteridophytic (2.62%) had higher values compared to the preceding pollen zones. Drifted pollen has very low values (1% pollen). Fungal spores are recorded in variable high-to-low values in this pollen zone too.

Thus, the dense mixed tropical deciduous forest became relatively denser from~ 1961 cal yr BP to the present under a warm and relatively more humid climate with a further increase in ISMR. Agricultural practice and other anthropogenic activities, however,

decreased comparatively. The lake, contrarily, became larger; however, swampy conditions prevailed. Pteridophytic fern spores also grew locally in moist and shady locations close to the lake. The scant presence of drifted pollen is indicative of its exclusive transportation by wind from the Himalayas.

4.2. Grain Size (Particle Size)

The various fractions of grain size along with their statistical parameters are plotted in Figure 5. The results for each phase are as follows:

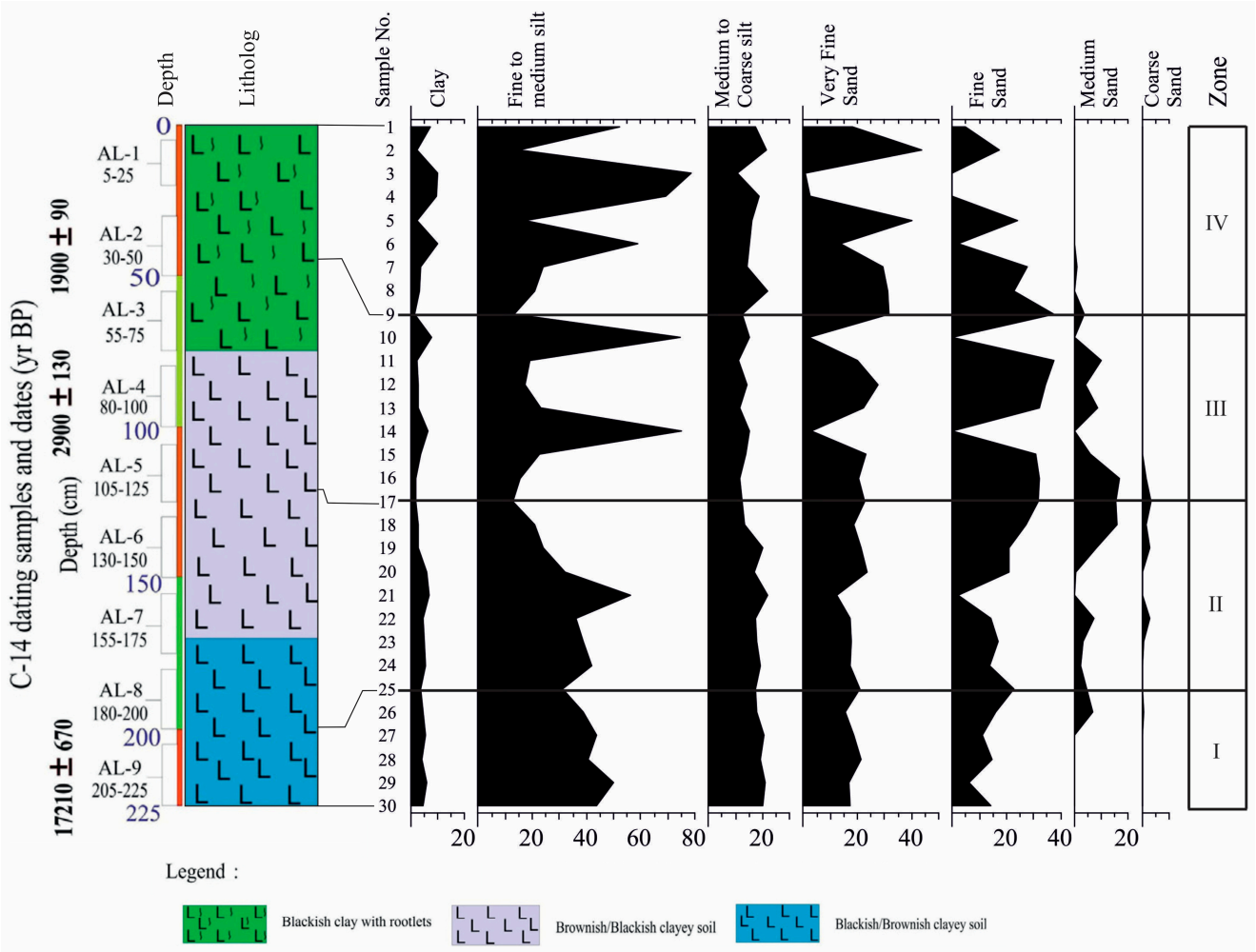

Figure 5. Diagram showing the variations in the various grain size parameters from the ANL, Koriya District of Chhattisgarh State, central Indian CMZ.

4.2.1. Zone I (~22,200–8658 cal yr BP)

During this deposition period, the clay fraction ranged from 4% to 6%, the silt fraction from 56% to 71% (with fine-to-medium silt contributing 38% to 49%) and the sand fraction from 23% to 39% (dominated by very fine and fine sand). Medium sand was present in low percentages, and coarse sand was less than 1% in PS-26 and absent in the other samples. The samples exhibited both unimodal and bimodal distributions, with mean grain sizes between 3∅ and 4∅. The sorting values ranged from 1.15∅ to 1.46∅, skewness was negative between −0.27∅ and −0.39∅, and kurtosis ranged from 0.74∅ to 1.05∅, indicating poorly sorted sediments with coarse-to-very-coarse skewed grains, which were either platykurtic or mesokurtic.

The samples' unimodal and bimodal distributions suggest deposition in low-energy environments, with an average mean grain size of 3.5∅, indicating fine-grained sediments.

The average sorting value of 1.26∅ suggests poor sorting. The sediments were negatively skewed, with an average skewness of −0.31∅, indicating a coarse and very coarse skewed distribution, reflecting unidirectional sediment transport. The mesokurtic character indicates deposition by unidirectional flow in a low-energy setting, while the platykurtic nature suggests the mixing of sediments from two sources.

4.2.2. Zone II (~18,658–7340 cal yr BP)

During this period, the clay content varied from 2% to 6%, with the silt and sand proportions being roughly equal. Silt ranged from 34% to 78%, with fine-to-medium silt mainly ranging from 20% to 56%, while medium-to-coarse silt ranged from 13% to 21%. The sand was mostly very fine to fine, with low-to-moderate amounts of medium and coarse sand. The sediments were both unimodal and bimodal, with mean grain sizes from 2∅ to 4∅ and sorting values from 1.05∅ to 1.57∅. The skewness values were mostly negative, except for that of PS-18, which was positive, and kurtosis ranged from 0.67∅ to 1.33∅.

The sediments, which were poorly sorted, reflected low-energy depositional conditions. The mean grain size averaged 3.2∅, indicating a fine-grained composition. The sorting values averaged 1.39∅, and skewness was mainly coarse to very coarse, with occasional symmetrical and fine-skewed samples. Negative skewness values suggested periods of erosion or non-deposition, with coarse skewness indicating unidirectional sediment transport. Most samples were platykurtic, suggesting fine-to-medium sand dominance, and were indicative of low-to-moderate energy depositional settings.

4.2.3. Zone III (~7340–1961 cal yr BP)

During this period, the clay content varied from 1% to 8%, silt from 25% to 90% (with fine-to-medium silt making up 12% to 75%), and sand from 2% to 73%. A high sand content appeared mainly in the lower part of the zone, with varying amounts of very fine, fine and medium sand, and coarse sand present in very low proportions. The samples showed both unimodal and bimodal distributions, with mean grain sizes from 2∅ to 5∅. The sorting values ranged from 0.69∅ to 1.50∅, and the skewness was mostly positive (ranging from −0.02∅ to 0.32∅) except for that of PS-14, which was negative. Kurtosis varied from 0.69∅ to 1.97∅. Most sediments were poorly sorted, except for PS-10 and PS-14, which were moderately sorted. The grains were generally fine-skewed, with PS-11 showing a very fine skewness and PS-14 being symmetrically skewed. Most samples were platykurtic, except for PS-10 and PS-14, which were very leptokurtic, and PS-17, which was mesokurtic.

The average mean grain size was 3∅, indicating fine-grained sediment. The sorting averaged 1.25∅, suggesting poor sorting overall, with one moderately sorted sample. The skewness was mostly positive, indicating low-to-moderate energy levels during deposition, with only one sample negatively skewed. Predominantly fine-skewed samples suggest a high level of winnowing or the long-distance transportation of sediments [85–87]. The mesokurtic and leptokurtic nature of some of the sediments suggests the addition of finer-sediment fractions. Skewness and kurtosis values indicate a low-energy riverine environment during deposition [88].

4.2.4. Zone IV (~1961 cal yr BP–Present)

During this period, silt content ranged from 25% to 89%, with a predominance of fine-to-medium silt and lower amounts of medium-to-coarse silt. The sand content varied from 0.6% to 73%, primarily consisting of very fine and fine sand, while the clay content ranged from 1% to 10%. Medium and coarse sand were negligible or absent. A grain size analysis using the Folk and Ward method indicated that the samples were either unimodal or bimodal, with mean grain sizes from 2∅ to 5∅. The sorting values ranged from 0.77∅ to 1.32∅, and skewness varied from −0.20∅ to +0.30∅. The kurtosis values ranged from 0.70∅ to 2.28∅. Most sediments were poorly sorted, with some moderately sorted, primarily fine-skewed, and a few coarse-skewed or symmetrical (PS-4). The kurtosis values ranged from platykurtic to very leptokurtic.

The unimodal sediments indicated a consistent deposition process and low-energy conditions. The mean grain sizes averaged 3.4∅, indicating fine-grained sediments [89,90]. A positive skewness suggested winnowing activity, while variations in skewness reflected low-to-moderate energy conditions. Fine and symmetrical skewness values indicated the deposition of finer fractions as coarser content was removed. The kurtosis values varied from mesokurtic to leptokurtic, indicating an increase in fine sediment fractions after winnowing, preserving the initial sediment character. Leptokurtic sediments suggested fluctuating energy conditions, while mesokurtic sediments indicated unidirectional flow and sediment settling in low-energy environments [85–88].

4.3. Eenvironmental Magnetism

The environmental magnetic parameters showing the magnetic concentration are plotted against depth and age in Figure 6. The mass specific magnetic susceptibility (χlf, which measures the total concentration of magnetic minerals present in a natural sample [69,73]) values vary between 60.21 and 781.57 $\times$ 10^{-8} m^3 kg^{-1} with an average of 219.96 $\times$ 10^{-8} m^3 kg^{-1} (Figure 6, Table S2). These χlf values are quite high with respect to the χlf values reported from the Ganga flood plains [74] due to the geology (Deccan traps) of the area [75–77]. The frequency-dependent susceptibility percentage (χfd%) indicates the proportion of superparamagnetic (SP) grains [78]. The χfd% values for the sediments vary from −2.74% (17.5 cm) to 3.05% (27.5 cm; Figure 6). The average χfd% value is 1.63% (Figure 6, Table S2). These values close to zero suggest the lack of SP magnetite grains of bacterial origin [75]. The susceptibility of anhysteretic remanent magnetization (χARM) is biased towards magnetic minerals of a stable single domain (SSD) grain size [70]. Values of χARM vary between 12.24 $\times$ 10^{-8} m^3 kg^{-1} (37.5 cm) and 1691.53 $\times$ 10^{-8} m^3 kg^{-1} (155 cm) with an average of 438.73 $\times$ 10^{-8} m^3 kg^{-1} (Figure 6, Table S2). Saturation isothermal remanent magnetization (SIRM) is generally influenced by the concentration of all remanence-carrying magnetic minerals [69] and, hence, reflects the total concentration of the remanence-carrying magnetic mineral content [76]. Values of the SIRM range between 762.97 $\times$ 10^{-5} Am^2 kg^{-1} (32.5 cm) and 17,796 $\times$ 10^{-5} Am^2 kg^{-1} (155 cm) with an average of 4373.04 $\times$ 10^{-5} Am^2 kg^{-1} (Figure 6, Table S2), suggesting a high concentration of magnetic minerals since 22,200 cal yr BP. The S-ratio, which is indicative of relative proportions of ferrimagnetic and antiferromagnetic minerals in the sample, varies between 0.95 and 1.00 [69,71]. A high value (~1) of the S-ratio (Figure 6, Table S2) indicates the presence of predominantly low-coerciveness, magnetically "soft" minerals like magnetite and maghemite, whereas lower S-ratio values refer to the presence of a mixedmineralogy of magnetite and anti-ferromagnetic minerals (haematite and goethite) in the samples. This supports the fact that the magnetic mineralogy of the sediment is dominated by ferromagnetic minerals like magnetite and maghemite. The HIRM values (Figure 6, Table S2) fluctuate between a low of 0.07 $\times$ 10^{-5} Am^2 kg^{-1} (27.5 cm) and a high of 310.31 $\times$ 10^{-5} Am^2 kg^{-1} (95 cm) with an average of 77.34 $\times$ 10^{-5} Am^2 kg^{-1}, suggesting a significant concentration of high-coerciveness magnetic minerals like hematite and goethite, though their relative contribution to remanent magnetisation is quite small. Roberts et al. [77] has reported that even an S-ratio of 0.90 suggests 90% hematite (wt%) in the sample matrix though its relative contribution to remanent magnetisation is reasonably small, largely because of its antiferromagnetic nature. The inter-parametric ratios, χARM/SIRM, SIRM/χlf and χARM/χlf, are used to determine the magnetic grain size qualitatively. High ratios of χARM/SIRM and χARM/χlf generally indicate a finer magnetic grain size and vice versa (Figure 6, Table S2) [76,78], whereas high ratios of SIRM/χlf suggest coarser grain size fractions and vice-versa.

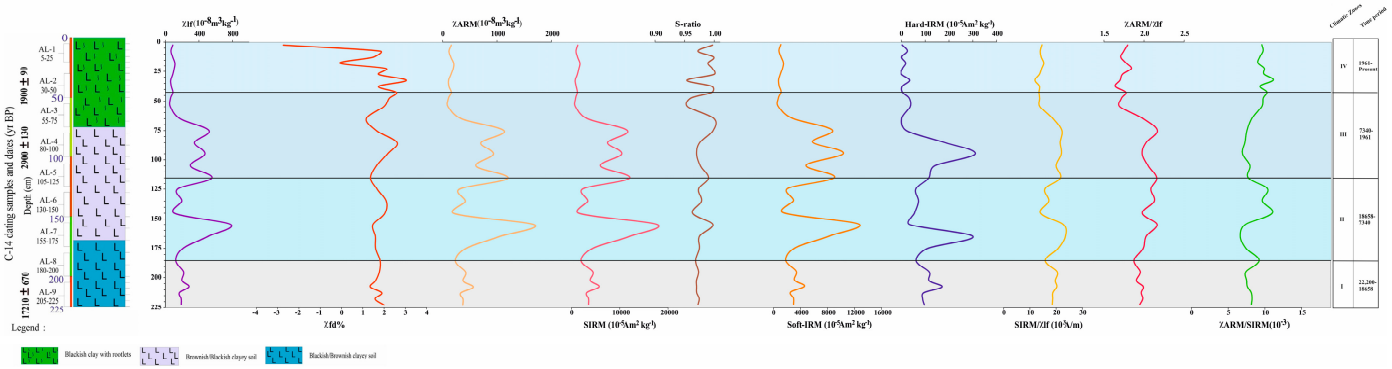

Figure 6. Diagram showing the variations in the various parameters of the environmental magnetism study from the ANL, Koriya District of Chhattisgarh State, central Indian CMZ.

Magnetic minerals in sediments can be derived from a variety of sources [69]. Apart from detrital input, bacterial magnetite [91], authigenicgreigite [92] and anthropogenic magnetite originating from industrial activities, automobile emissions and so on [93] may all contribute to sediment magnetism. Furthermore, the diagenetic dissolution of magnetic minerals owing to organic matter breakdown is a possibility [94]. Low values of $\chi_{ARM}/\chi lf$ throughout the ANL profile in the current study discard the involvement of bacterial magnetite in sediments [75]. Likewise, lower SIRM/χlf ratios below the greigite threshold value (i.e., 40×10^3 Am^{-1}; [92]) further rule out the occurrence of iron sulphide in the ANL sediments. Additionally, the inter-parametric ratios (indicative of magnetic grain size) such as $\chi_{ARM}/\chi lf$ and χ_{ARM}/SIRM do not show significant changes along the profile, indicating that magnetic dissolution had no effect on the magnetic record [78].

The correlation coefficient matrix (Supplementary Table S1) shows strong correlations of χlf with the other concentration-dependent parameters of χARM, SIRM and Soft-IRM, revealing the dominant ferrimagnetic nature of the magnetic minerals. The overall strong correlation of χlf with SIRM/χlf (r2 = 0.85) suggests the coarser magnetic grain sizes of magnetite/maghemite as major remanence-carrying minerals, and the significant correlation of χlf with χARM/χlfi.e (r2 = 0.45) suggests relatively finer grain sizes of magnetite/maghemite as remanence-carrying minerals as can be observed in patches.As the samples are well saturated within a field value of 300 mT (with an S-ratio close to 1), a poor correlation of the S-ratio with the other parameters is observed.

4.3.1. Zone I (~22,200–18,658 cal yr BP)

It is observed that Zone I is characterised by a stable yet low concentration of a ferrimagnetic mineral input of coarser magnetic grain sizes as the ratios of χARM/SIRM andχARM/χlf are relatively low and the SIRM/χlf values are higher in this zone. An overall strong correlation of χlf is observed in the entire profile with the concentration-dependent metrics of ARM, SIRM and Soft-IRM showing ferrimagnetic minerals, such as magnetite and maghemite as dominant remanence carriers. A very strong correlation of χlfwith SIRM/χlf and a strong correlation of Soft-IRM with SIRM/χlf suggest the coarser nature of the ferrimagnetic mineral assemblages.

4.3.2. Zone II (~18,658–7340 cal yr BP)

This zone is characterized with fluctuating concentrations of magnetic mineral input with the highest magnetic concentration values occurring at a depth of ~155 cm, which certainly decreased at shallower depths (~125 cm). Therefore, both coarser and finer magnetic grain sizes are observed in this zone. The major remanence-carrying mineral is coarser and finer magnetite/maghemite. A similar observation of the sediment particle size transition can be inferred from the fine-to-medium silt fraction. The coarser grain fraction is corresponding well with the concentration-dependent metrics of χlf, ARM, SIRM and

Soft-IRM. The overall environmental magnetic parameters depict a fluctuating trend with high rainfall conditions in the region.

4.3.3. Zone III (~7340–1961 cal yr BP)

The lower part of this zone exhibits a high magnetic mineral concentration as shown by χlf, SIRM and χARM values. Overall, this zone is characterised with a high yet fluctuating concentration of magnetic mineral input together with predominant ferrimagnetic magnetite or maghemite mineral of a finer grain size range as evident from the ratio parameters. The pollen assemblage during this time period indicates increased frequencies of tree taxa, suggesting comparatively dense forests in the study area. Therefore, when there were high amounts of rainfall, the forests barred the coarse-grain sediments from reaching the lake, leading to the deposition of high amounts of silt and fine sand particles, which is well represented in the grain size parameters as well [74].

4.3.4. Zone IV (~1961 cal yr BP–Present)

This zone shows a relatively low and stable concentration of magnetic minerals of fine grain sizes as evident from low values of χlf, ARM, SIRM and Soft-IRM and grain size proxies of ratio parameters. Overall, a decline in the magnetic parameters implies reduced sediment transport to the lake attributed to increased/dense vegetation [74].

5. Synthesis of Pollen, Grain Size and Environmental Magnetism Data: Global Contextualization and Forcing Factors

Pollen records demonstrate that between ~22,200 and 18,658 cal yr BP, open vegetation occupied the landscape under a dry climate, probably indicating reduced ISMR (Table 2). The grain size data suggest that fine-grained sediment deposition occurred with two sources, which was directly correlated to the lower ISMR. Moreover, the concentration-dependent parameters, such as χlf, χARM and SIRM, exhibit low values during this period. Therefore, several pieces of evidence such as those above are suggestive of low ISMR conditions in the study area. The low ISMR during ~22,200–18,658 cal yr BP is globally correlated with the Last Glacial Maximum (LGM) (Figure 7) [95]), which corresponds to changes in the following: particular orbital patterns(i.e., the precession cycle), albedo, the NH ice sheet, CO_2, CH_4, other greenhouse gases (e.g., water vapour) and the warming of the Pacific Ocean. These led to an increase in summer insolation near the tropics, which resulted in enhanced atmospheric water transport from the sea [96–102]. Duplessy [103] suggested lower ISMR during the LGM in the Bay of Bengal (BoB), based on the observed $\delta^{18}O$ enrichment in planktonic foraminifera, which led to the reduced influx of fresh water into the BoB. A prominent rainfall minimum during ~20 ka was observed in the Ganga Plain, India [104–106]. A cool and dry climate (reduced ISMR) was suggested between 21,000 and 18,000 cal yr BP, which supported the open grassland type of vegetation in the Ganga Plain during the LGM [107]. The LGM was also noticed in Central India [108], the South Indian Mountains [109] and the Eastern Himalayas [110]. Wasson et al. [111] also reported the LGM in the Sambhar Lake of the Thar Desert Rajasthan, India to be ~21,000 cal yr BP. A cold and dry climate in response to low ISMR was suggested on the basis of high-resolution stable isotopic ($\delta^{18}O$ and $\delta^{13}C$) as well as glycerol dialkyl glycerol tetraether (GDGT) studies conducted on stalagmite during the LGM from Mawmluh Cave (Meghalaya), Northeastern India [112], resulting in reduced vegetation (as exhibited by high $\delta^{13}C$ values). A cool and dry climate during the LGM was suggested in Darjeeling, Eastern Himalaya, India [110]. A declining monsoon, which transformed forests into savannahs under a cooler and drier climate during the LGM, was inferred from the Ziro Valley of Arunachal Pradesh, Eastern Himalayas, India [113]. Drier climatic conditions can be inferred from a sharp drop in the ratio of evergreen to deciduous elements, corresponding to an abrupt rise in non-arboreals (herbaceous vegetation) and a sharp decline in arboreal percentages (trees and shrubs) during the LGM (~22.3–18.3 ka), as observed in the Darjeeling foothill region, Eastern Himalayas [114]. A weak monsoon has also been inferred in Kumaun, Central Himalayas,

India, during the LGM [115]. Premathilake and Risberg [116] and Premathilake [117] suggested a semi-arid climate affected by cool and dry conditions owing to low ISMR during the LGM in Sri Lanka. Zhang et al. [118] suggested a dry climate and decreased ISMR as manifested by abundant C4 plants in the terrestrial ecosystem around Lake Lugu between 30 and 14.6 ka in Southwest China (the ISM region). The strengthening of the westerlies and their shift southwards–eastwards during the LGM have been suggested; however, based on lacustrine studies in West China, there was a moderate or high water level [119]. Clement et al. [96] and Overpeck et al. [8] suggested a very weak monsoon, accompanied by cool global temperatures during the LGM in the Indian subcontinent and the Arabian Sea, respectively. In the Arabian Sea, reduced in situ productivity [120–122], reduced denitrification [100] and a lower sea-surface temperature (SST) [100,123] have been suggested. Similarly, a reduced SST [124,125] with enriched foraminiferal $\delta^{18}O$ values [126–128], depleted sea water $\delta^{18}O$ [129], reduced detrital contribution [130] and reduced calcareous productivity [131] have been suggested in the Bay of Bengal. However, a higher level of calcareous productivity during the LGM has been suggested from the northern part of the Bay of Bengal, attributed to the monsoon-triggered river discharges that led to the dilution of $CaCO_3$ content in the sediments during the interglacial period and vice-versa during the glacial time [132]. The microparticle concentration increased after 25 ka and reached a peak during 20–15 ka in the Guliya ice cap, China [133], whichsupports increased dust emissions and the expansion of Central Asian dust realms during the LGM [134].

Table 2. Rainfall marker taxa and their rainfall (annual) requirements (Champion and Seth, 1968) [53].

Rainfall Marker Taxa	Rainfall (Annual) Requirements
Tropical evergreen forest elements: *Syzygium cumini*, *S. heyneanum*, *Barringtonia* sp.	>2000 mm
Tropical semi-evergreen forest element(s): *Shorea robusta*	1600–1900 mm
Tropical moist deciduous elements: *Madhuca indica*, *Terminalia*, *Schleichera*, *Eucalyptus*, *Adina cordifolia*, *Mitragyna parvifolia*, *Grewia*, *Mallotus philippensis*, *Mimusops elangi*, *Manilkara hexandra*	1500–2000 mm (1250–1900 mm)
Tropical dry deciduous forest elements: *Lannea coromandelica*, *Lagerstroemia parvifolia*, *Emblica officinalis*, *Aegle marmelos*, *Tectona grandis*, *Bombax ceiba*, *Acacia* sp., *Diospyros melanoxylon*, *Semecarpus anacardium*, *Buchanania lanzan*	1250–750 mm

Between ~18,658 and 7340 cal yr BP, the ISMR comparatively increased and supported open mixed tropical deciduous forests under a warm and moderately humid climate (Table 2, Figure 7). The varying degrees of the grain size parameters, such as fine- and medium-grain sediments during the depositional period, indicate local as well as long-distance sediment transport and winnowing activity owing to a comparatively increased level of ISMR. The environmental magnetic parameters also depict increased rainfall conditions as the values of χlf, χARM, SIRM and HIRM are considerably higher during the early part of this phase. This suggests that the mineralogical parameters are in accordance with the palynological and grain size results concerning the ISMR variability. A large degree of climatic amelioration with a significant rise in SWM rains between 10,400 and 9850 cal yr BP was reported in Sri Lanka [135]. An orbitally induced increment of summer insolation triggered the strengthening of the ISM [116]. Nevertheless, the time span during 11.7–6 ka also included abrupt climatic episodes of relatively weaker ISMs, which can be linked with the North Atlantic climate [136,137]. The microparticle concentration in the Guliya ice cap in the Tibetan Plateau was significantly lower during 11–8 ka throughout the Holocene epoch, suggesting a prominent decline in atmospheric dust and an intensification

of the summer monsoon [133]. The strengthened SWM rains seem to have shown positive correlations with the high level of insolation in NH, warm conditions in the North Atlantic climate and ENSO-like conditions [138–140]. The high level of insolation might have caused the increased rainfall, and the paleoclimatic record from the central Indian CMZ may support this notion [26].

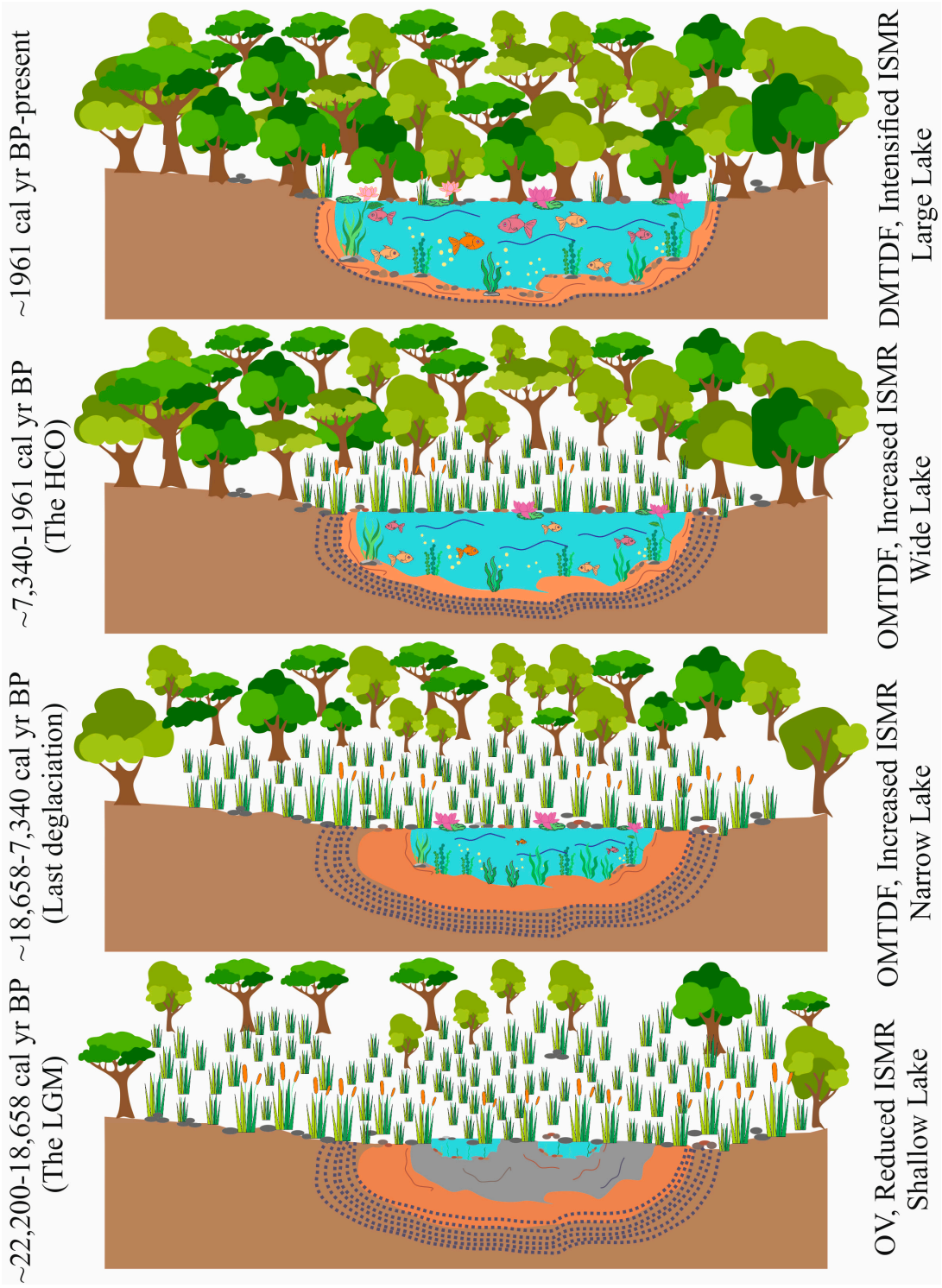

Figure 7. Schematic diagram showing the evolution of the sedimentary environment (lake-level changes), as well as vegetation (dynamics) and the ISMR variability since the LGM in the central Indian CMZ. (OV = open vegetation; OMTDF: open mixed tropical deciduous forest; DMTDF: dense mixed tropical deciduous forest; LGM = Last Glacial Maximum; HCO = Holocene Climate Optimum).

Subsequently, between ~7340 and 1961 cal yr BP, open mixed tropical deciduous forests continued to grow in the study area with some increase in the prominent tree taxa under a warm and relatively more humid climate with comparatively increased ISMR (Table 2). The grain size shows fine-grained sediments, indicating high winnowing activity, which is suggestive of low-energy riverine or local erosion activity. This time period is characterized by high values of magnetic parameters such as χlf, χARM and SIRM, suggesting coarser material due to comparatively dense vegetation (the tree frequency increased), which indicates that increased ISMR conditions prevailed during this time period. Also, low erosion activity even during the high ISMR conditions has beensuggested during this period, which could be due to the dense vegetation around the landscape of the study area. This instance of the amelioration of climatic conditions, from a global perspective, corresponds with the Holocene Climatic Optimum (HCO) (Figure 7), which falls broadly within the time interval of 7000–4000 BP [118]. A steady increase in the ISM intensity between 6.3 and 5.6 ka, based on $\delta^{18}O$ records in a stalagmite, was observed from the Kotumsar Cave in Chhattisgarh State (central India) [141]. An active SW monsoon during 10,000–5800 ^{14}C yr BP from the Ganga Plain was also inferred, corresponding to the early Mid-Holocene Climatic Optimum (HCO) [142]. An active SW monsoon during the HCO was also reported from different regions of India, such as Son Valley in North and central India [143] and Rajasthan in Western India [144–147]. However, the timing and magnitude of the HCO varies globally; i.e., it is asynchronous, which is why different names, such as the Holocene Thermal Maximum (HTM), Holocene Megathermal, Altithermal, Hypsithermal, Mid-Holocene Warm Period, Climatic Optimum and Holocene Optimum, have been proposed by different authors. Nonetheless, it is well established that the HCO was a relatively warm climatic phase between 11 and 5 ka BP [148–154]. This warming is commonly associated with the orbitally forced summer insolation maximum [155–157]. The HCO was affected by other forcings and feedbacks, as well as the remnant of the Laurentide ice sheet (LIS) [149,153]. Moreover, as far as the timings and magnitudes of maximum warming are concerned, these vary substantially among the different regions across the globe [154–157]. Finally, since 1961 cal yr BP onwards, the open mixed tropical deciduous forest has been succeeded by dense mixed tropical deciduous forest under a warm and relatively more humid climate with a further increase in the ISMR (Table 2; Figure 7). On the contrary, a decline in the magnetic parameters is recorded during this time period attributed to reduced sediment transport owing to increased vegetation, which barred the coarser sediments from reaching the lake [74].

6. Conclusions

Our multi-proxy approach (considering pollen, grain size and environmental magnetism) has suggested the evolution of ISMR variability since the LGM in the central Indian CMZ. The following conclusions can be drawn in the present study:

1. A reduced (weak) monsoon between ~22,200 and 18,658 cal yr BP (during the LGM) was suggested, which supported open vegetation in the landscape under a cool and dry climate. The presence of organic-deficient fine clay also confirms poor vegetation coverage and the influx of terrigenous material in the lake under low-energy conditions (low levels of rainfall). The magnetic concentration-dependent parameters (χ_{lf}, χARM, SIRM, S-ratio and Soft IRM) are also related to the lower ISMR.
2. Between ~18,658 and 7340 cal yr BP, the open vegetation was replaced by open mixed tropical deciduous forest under a warm and moderately humid climate, indicating increased monsoon rainfall. A comparatively increased level of floristic diversity is marked by the rise in organic matter generated by the degradation of biomass accumulated on the forest floor. Moreover, the increasing trend in environmental magnetic parameters, such as χ_{lf}, χARM, SIRM and grain size data (high-energy condition), also support a warm and moderately humid climate during this phase.
3. Between ~7340 and 1961 cal yr BP, comparatively increased levels of monsoon rainfall supported open mixed tropical deciduous forest in the study area with an increase in

some other tree taxa under a warm and humid climate. The climate, thus, was ameliorated, which could be globally correlated with the HCO. The increasing trend in the environmental magnetic parameters and the grain size data (high-energy conditions) also supports a warm/humid climate reducing the severity of the monsoon during this phase.

4. The level of monsoon rainfall increases comparatively from ~1961 cal yr BP to the present, and mixed tropical deciduous forest succeeds the open mixed tropical deciduous forest under a warm and more humid climate. The environmental magnetic parameters and the grain size data corroborate the palynogical findings of this phase on the ISMR variability.
5. The trends in agricultural practice as well as lake-level changes are in agreement with the variations in the ISMR.

Our study shows that the vegetation history, climate changes and monsoonal variability in the central Indian CMZ were controlled by the NH summer insolation and ice sheet dynamics and were also influenced by the sea surface temperature of the Indian Ocean.

Supplementary Materials: The following supporting information can be downloaded at: https://www.mdpi.com/article/10.3390/quat7040052/s1, Table S1. Showing the correlation coefficient matrix of the observed magnetic parameters. Table S2. Variations of environmental magnetic parameters along the ANL supplementary archive.

Author Contributions: Conceptualization, M.F.Q., J.D., B.T. and S.J.S.; methodology, N.P., M.J., P.T. and M.E.T.M.; formal analysis, M.F.Q., J.D., N.P., M.J., P.K.D., P.T. and M.E.T.M.; investigation, M.F.Q., J.D., N.P., M.J., P.K.D., P.T. and M.E.T.M.; data curation, M.F.Q., J.D., N.P., M.J., P.K.D., P.T. and M.E.T.M.; writing—original draft preparation, M.F.Q., J.D. and B.T.; writing—review and editing, M.F.Q., J.D. and B.T.; visualization, M.F.Q., J.D. and B.T.; supervision, M.F.Q., J.D., B.T. and S.J.S. All authors have read and agreed to the published version of the manuscript.

Funding: The Birbal Sahni Institute of Palaeosciences (BSIP), Lucknow (Uttar Pradesh), India Department of Science and Technology (DST), Ministry of Science & Technology, Government of India, New Delhi, India funded this study. The present research is an outcome of the Institute Project (Project Component No. 8: BSIP/RDCC/2021-2025/8).

Data Availability Statement: The data that support the findings of this study are available from the corresponding author upon request.

Acknowledgments: We are thankful to the Director, Birbal Sahni Institute of Palaeosciences, Lucknow, India for providing the facilities needed to conduct this study and giving us permission to publish our results.

Conflicts of Interest: The authors declare no conflicts of interest.

References

1. Parthasarathy, B.; Pant, G.B. The spatial and temporal relationships between the Indian summer monsoon rainfall and the Southern Oscillation. *Tellus. Ser. A Dyn. Meteorol. Oceanogr.* **1984**, *36*, 269–277.
2. Meehl, G.A. Coupled land-ocean-atmosphere processes and South Asian monsoon variability. *Science* **1994**, *266*, 263–267. [CrossRef] [PubMed]
3. Wang, B.; Fan, Z. Choice of South Asian summer monsoon indices. *Bull. Am. Meteorol. Soc.* **1999**, *80*, 629–638. [CrossRef]
4. Hu, Z.Z.; Latif, M.; Roeckner, E.; Bengtsson, L. Intensified Asian summer monsoon and its variability in a coupled model forced by increasing greenhouse gas concentrations. *Geophys. Res. Lett.* **2000**, *27*, 2681–2684. [CrossRef]
5. Wang, B. *The Asian Monsoon*; Springer Science & Business Media: Berlin/Heidelberg, Germany, 2006.
6. Wang, Y.J.; Cheng, H.; Edwards, R.L.; He, Y.; Kong, X.; An, Z.; Wu, J.; Kelly, M.J.; Dykoski, C.A.; Li, X. The Holocene Asian monsoon: Links to solar changes and North Atlantic climate. *Science* **2005**, *308*, 854–857. [CrossRef]
7. Hernandez, M.; Ummenhofer, C.C.; Anchukaitis, K.J. Multi-scale drought and ocean atmosphere variability in monsoon Asia. *Environ. Res. Lett.* **2015**, *10*, 074010. [CrossRef]
8. Overpeck, J.; Anderson, D.; Trumbore, S.; Prell, W. The southwest Indian monsoon over the last 18,000 years. *Clim. Dyn.* **1996**, *12*, 213–225. [CrossRef]
9. Pant, G.B.; Rupa Kumar, K. *Climates of South Asia*; John Wiley and Sons: New York, NY, USA, 1997.

10. Webster, P.J.; Magana, V.O.; Palmer, T.N.; Shukla, J.; Tomas, R.A.; Yanai, M.U.; Yasunari, T. Monsoons: Processes, predictability, and the prospects for prediction. *J. Geophys. Res. Oceans* **1998**, *103*, 14451–14510. [CrossRef]
11. Gadgil, S. The Indian monsoon and its variability. *Am. Rev. Earth Planet. Sci.* **2003**, *31*, 429–467. [CrossRef]
12. Gadgil, S.; Gadgil, S. The Indian monsoon, GDP and agriculture. *Econ. Polit. Wkly.* **2006**, *41*, 4887–4895.
13. Misra, P.; Farooqui, A.; Sinha, R.; Khanolkar, S.; Tandon, S.K. Millennial-scale vegetation and climatic changes from an Early to Mid-Holocene lacustrine archive in Central Ganga Plains using multiple biotic proxies. *Quat. Sci. Rev.* **2020**, *243*, 106474. [CrossRef]
14. Kumar, K.K.; Rajagopalan, B.; Cane, M.A. On the weakening relationship between the Indian monsoon and ENSO. *Science* **1999**, *284*, 2156–2159. [CrossRef] [PubMed]
15. Krishnamurthy, V.; Goswami, B.N. Indian monsoon-ESNO relationship on interdecadal timescale. *J. Clim.* **2000**, *13*, 569–595. [CrossRef]
16. Ghosh, S.K.; Pant, M.C.; Dewan, B.N. Influence of the Arabian Sea on the Indian summer monsoon. *Tellus* **1978**, *30*, 117–125. [CrossRef]
17. Wright, R.P.; Bryson, R.; Schuldenrein, J. Water supply and history: Harappa and the Beas regional survey. *Antiquity* **2008**, *82*, 37–48. [CrossRef]
18. Kale, V.S.; Gupta, A.; Singhvi, A.K. Late Pliestocene-Holocene paleohydrology of Monsoon Asia. In *Paleohydrology: Understanding Global Change*; Gregory, K.J., Benito, G., Eds.; John Wiley and Sons: New York, NY, USA, 2003; pp. 213–232.
19. Staubwasser, M.; Sirocko, F.; Grotes, P.; Segl, M. Climate change at the 4.2 ka BP termination of the Indus valley civilization and Holocene south Asian monsoon variability. *Geophys. Res. Lett.* **2003**, *30*, 1425. [CrossRef]
20. Zhang, P.; Cheng, H.; Edwards, R.L.; Chen, F.; Wang, Y.; Yang, X.; Liu, J.; Tan, M.; Wang, X.; Liu, J.; et al. A test of climate, sun, and culture relationships from an 1810-year Chinese cave record. *Science* **2008**, *322*, 940–942. [CrossRef]
21. Buckley, B.M.; Anchukaitis, K.J.; Penny, D.; Fletcher, R.; Cook, E.R.; Sano, M.; Le, C.N.; Wichienkeeo, A.; Minh, T.T.; Marcus, H.J. Climate as a contributing factor in the demise of Angkor, Cambodia. *Proc. Natl. Acad. Sci. USA* **2010**, *107*, 6748–6752. [CrossRef]
22. Cook, E.R.; Anchukaitis, K.J.; Buckley, B.M.; D'Arrigo, R.D.; Jacoby, G.C.; Wright, W.E. Asian monsoon failure and mega drought during the last millennium. *Science* **2010**, *328*, 486–489. [CrossRef]
23. Wasson, R.J.; Sundriyal, Y.P.; Chaudhary, S.; Jaiswal, M.K.; Morthekai, P.; Sati, S.P.; Juyal, N. A 1000-year history of large floods in the Upper Ganga catchment, central Himalaya, India. *Quat. Sci. Rev.* **2013**, *77*, 156–166. [CrossRef]
24. Leipe, C.; Demske, D.; Tarasov, P.E.; Wünnemann, B.; Riedel, F.; HIMPAC Project members. A Holocene pollen record from the northwestern Himalayan lake Tso Moriri: Implications for palaeoclimatic and archaeological research. *Quat. Int.* **2014**, *348*, 93–112. [CrossRef]
25. Dixit, Y.; Hodell, D.A.; Petrie, C.A. Abrupt weakening of the summer monsoon in Northwest India ~4100 yr ago. *Geology* **2014**, *42*, 339–342. [CrossRef]
26. Gupta, A.K.; Anderson, D.M.; Overpeck, J.T. Abrupt changes in the Asian southwest monsoon during the Holocene and their links to the North Atlantic Ocean. *Nature* **2003**, *421*, 354–357. [CrossRef] [PubMed]
27. Gupta, A.K.; Anderson, D.M.; Pandey, D.N.; Singhvi, A.K. Adaptation and human migration, and evidence of agriculture coincident with changes in the Indian summer monsoon during the Holocene. *Curr. Sci.* **2006**, *90*, 1082–1090.
28. Saraswat, R.; Nigam, R.; Correge, T. A glimpse of the Quaternary monsoon history from India and adjoining seas. *Palaeogeogr. Palaeoclimatol. Palaeoecol.* **2014**, *397*, 1–6. [CrossRef]
29. Srivastava, G.; Trivedi, A.; Mehrotra, R.C.; Paudayal, K.N.; Limaye, R.B.; Kumaran, K.P.N.; Yadav, S.K. Monsoon variability over Peninsular India during Late Pleistocene: Signatures of vegetation shift recorded in terrestrial archive from the corridors of Western Ghats. *Palaeogeogr. Palaeoclimatol. Palaeoecol.* **2016**, *443*, 57–65. [CrossRef]
30. Cai, Y.; Tan, L.; Cheng, H.; An, Z.; Edward, R.L.; Kelly Megan, J.; Kong, X.; Wang, X. The variation of summer monsoon precipitation in central China since the last deglaciation. *Earth Planet. Sci. Lett.* **2010**, *291*, 21–31. [CrossRef]
31. Singhvi, A.K.; Rupakumar, K.; Thamban, M.; Gupta, A.K.; Kale, V.S.; Yadav, R.R.; Bhattacharyya, A.; Phadtare, N.R.; Roy, P.D.; Chauhan, M.S.; et al. Instrumental, terrestrial and marine records of the climate of South Asia during the Holocene: Present status, unresolved problems and societal aspects. In *Global Environmental Changes in South Asia: A Regional Perspective*; Springer: Dordrecht, The Netherlands, 2010; pp. 54–124.
32. Misra, V.; Mishra, A.; Bhardwaj, A. Simulation of the intraseasonal variations of the Indian summer monsoon in a regional coupled ocean–atmosphere model. *J. Clim.* **2018**, *31*, 3167–3185. [CrossRef]
33. Thamban, M.; Kawahata, H.; Rao, V.P. Indian summer monsoon variability during the Holocene as recorded in sediments of the Arabian Sea: Timing and implications. *J. Oceanogr.* **2007**, *63*, 1009–1020. [CrossRef]
34. Naik, S.S.; Godad, S.P.; Naidu, P.D.; Tiwari, M.; Paropkari, A.L. Early- to late Holocene contrast in productivity, OMZ intensity and calcite dissolution in the eastern Arabian Sea. *Holocene* **2014**, *24*, 749–755. [CrossRef]
35. Saraswat, R.; Naik, D.K.; Nigam, R.; Gaur, A.S. Timing, cause and consequences of mid-Holocene climate transition in the Arabian Sea. *Quat. Res.* **2016**, *86*, 162–169. [CrossRef]
36. Khan, H.; Govil, P.; Panchang, R.; Agrawal, S.; Kumar, P.; Kumar, B.; Verma, D. Surface and thermocline ocean circulation intensity changes in the western Arabian Sea during∼ 172 kyr. *Quat. Sci. Rev.* **2023**, *311*, 108133. [CrossRef]

37. Prasad, S.; Anoop, A.; Riedel, N.; Sarkar, S.; Menzel, P.; Basavaiah, N.; Krishnan, R.; Fuller, D.; Plessen, B.; Gaye, B.; et al. Prolonged monsoon droughts and links to Indo-Pacific warm pool: A Holocene record from Lonar Lake, central India. *Earth Planet. Sci. Lett.* **2014**, *391*, 171–182. [CrossRef]
38. Rawat, S.; Gupta, A.K.; Sangode, S.J.; Srivastava, P.; Nainwal, H.C. Late Pleistocene–Holocene vegetation and Indian summer monsoon record from the Lahaul, Northwest Himalaya, India. *Quat. Sci. Rev.* **2015**, *114*, 167–181. [CrossRef]
39. Quamar, M.F.; Kar, R.; Thakur, B. Vegetation response to the Indian Summer Monsoon (ISM) rainfall variability during the Late Holocene from the central Indian Core Monsoon Zone. *Holocene* **2021**, *31*, 1197–1211. [CrossRef]
40. Kar, R.; Quamar, M.F. Pollen-based Quaternary palaeoclimatic studies in India: An overview of the recent advances. *Palynology* **2019**, *43*, 76–93. [CrossRef]
41. Kar, R.; Quamar, M.F. Late Pleistocene-Holocene vegetation and climate change from the Western and Eastern Himalaya (India): Palynological perspective. *Curr. Sci.* **2020**, *119*, 195–218. [CrossRef]
42. Yadava, M.G.; Ramesh, R.; Pant, G.B. Past monsoon rainfall variations in peninsular India recorded in a 331-year-old speleothem. *Holocene* **2004**, *14*, 517–524. [CrossRef]
43. Sinha, A.; Cannariato, K.G.; Stott, L.D.; Cheng, H.; Edwards, L.; Yadava, M.G.; Ramesh, R.; Singh, I.B. A 900-year (600 to 1500 A.D.) record of the Indian summer monsoon precipitation from the core monsoon zone of India. *Geophys. Res. Lett.* **2007**, *34*, L16707. [CrossRef]
44. Kathayat, G.; Cheng, H.; Sinha, A.; Berkelhammer, M.; Zhang, H.; Duan, P.; Li, H.; Li, X.; Ning, Y.; Edwards, R.L. Evaluating the timing and structure of the 4.2 ka event in the Indian summer monsoon domain from an annually resolved speleothem record from Northeast India. *Clim. Past* **2018**, *14*, 1869–1879. [CrossRef]
45. Borgaonkar, H.P.; Sikder, A.B.; Ram, S.; Pant, G.B. El Niño and related monsoon drought signals in 523-year-long ring width records of teak (*Tectona grandis* L.F.) trees from south India. *Palaeogeogr. Palaeoclimatol. Palaeoecol.* **2010**, *285*, 74–84. [CrossRef]
46. Bhattacharyya, A.; Dhyani, R.; Joshi, R.; Shekhar, M.; Kuniyal, J.C.; Ranhotra, P.S.; Singh, S.P. Is survival of Himalayan Cedar (*Cedrus deodara*) threatened? An evaluation based on predicted scenarios of its growth trend under future climate change. *Sci. Total Environ.* **2023**, *882*, 163630. [CrossRef] [PubMed]
47. Kaushik, A.; Gupta, A.K.; Clemens, S.C.; Kumar, P.; Sanyal, P.; Gupta, P.; Pawar, R. Paleoclimatic reconstruction of northwest Himalaya since CE 475 using lake sediments from TadagTaal, Kumaun, India. *Palaeogeogr. Palaeoclimatol. Palaeoecol.* **2023**, *619*, 111544. [CrossRef]
48. Quamar, M.F.; Mir, I.A.; Jaiswal, J.; Bharti, N.; Dabhi, A.J.; Bhushan, R.; Prasad, N.; Javed, M. Hydro-climatic variability and consequent vegetation response during CE 1219-1942 from the Western Ghats, India. *Catena* **2023**, *232*, 107448. [CrossRef]
49. Quamar, M.F.; Bera, S.K. Pollen records of vegetation dynamics, climate change and ISM variability since the LGM from Chhattisgarh State, central India. *Rev. Palaeobot. Palynol.* **2020**, *278*, 104237. [CrossRef]
50. Köppen, W. Das geographische System der Klimate. In *Handbuch der Klimatologie*; Köppen, W., Geiger, R., Eds.; GebrüderBorntraeger: Berlin, Germany, 1936; pp. 1–44.
51. Quamar, M.F.; Kar, R. Modern pollen dispersal studies in India: A detailed synthesis and review. *Palynology* **2020**, *44*, 217–236. [CrossRef]
52. Harris, I.; Jones, P.D.; Osborn, T.J.; Lister, D.H. Updated high-resolution grids of monthly climatic observations-the CRU TS 3.10. *Int. J. Climatol.* **2014**, *34*, 623–642. [CrossRef]
53. Champion, H.G.; Seth, S.K. *A Revised Survey of Forest Types of India*; Manager of Publications, Government of India Press: New Delhi, India, 1968.
54. Reimer, P.J.; Bard, E.; Bayliss, A.; Beck, J.W.; Blackwell, P.G.; Bronk Ramsey, C.; Buck, C.E.; Cheng, H.; Edwards, R.L.; Friedrich, M.; et al. IntCal13 and MARINE13 radiocarbon age calibration curves 0–50,000 cal years BP. *Radiocarbon* **2013**, *55*, 1869–1887. [CrossRef]
55. Bronk Ramsey, C. Development of the radiocarbon calibration program. *Radiocarbon* **2001**, *43*, 355–363. [CrossRef]
56. Bronk Ramsey, C. Deposition models for chronological records. *Quat. Sci. Rev.* **2008**, *27*, 42–60. [CrossRef]
57. Blaauw, M.; Christen, J.A. Flexible paleoclimate age-depth models using an autoregressive gamma process. *Bayesian Anal.* **2011**, *6*, 457–474. [CrossRef]
58. Erdtman, G. *An Introduction to Pollen Analysis*; ChronicaBotanica: Waltham, MA, USA, 1943.
59. Chauhan, M.S.; Bera, S.K. Pollen morphology of some important plants of tropical deciduous sal (*Shorea robusta*) forests, district Sidhi, Madhya Pradesh. *Geophytology* **1990**, *20*, 30–36.
60. Chauhan, M.S.; Quamar, M.F. Vegetation and climate change in southeastern Madhya Pradesh during late Holocene, based on pollen evidence. *J. Geol. Soc. India* **2010**, *76*, 143–150. [CrossRef]
61. Nayar, T.S. *Pollen Flora of Maharashtra State, India*; Today and tomorrow's Printers and Publishers: New Delhi, India, 1990.
62. Quamar, M.F.; Chauhan, M.S. Late Quaternary vegetation, climate as well as lake-level changes and human occupation from Nitaya area in Hoshangabad District, southwestern Madhya Pradesh (India), based on pollen evidence. *Quat. Int.* **2012**, *263*, 104–113. [CrossRef]
63. Quamar, M.F.; Bera, S.K. Pollen records related to vegetation and climate change from northern Chhattisgarh, central India during the late Quaternary. *Palynology* **2017**, *41*, 17–23. [CrossRef]
64. Quamar, M.F.; Kar, R. Prolonged warming over the last ca. 11,700 years from the central Indian Core Monsoon Zone: Pollen evidence and a synoptic overview. *Rev. Palaeobot. Palynol.* **2020**, *276*, 104159. [CrossRef]

65. Vaasma, T. Grain-size analysis of lacustrine sediments: A comparison of pretreatment methods. *Estonian J. Ecol.* **2008**, *57*, 231–243. [CrossRef]
66. Udden, J.A. Mechanical composition of clastic sediments. *Geolog. Soc. Am. Bull.* **1914**, *25*, 655–744. [CrossRef]
67. Wentworth, C.K. A scale of grade and class terms for clastic sediments. *J. Geolog.* **1922**, *30*, 377–392. [CrossRef]
68. Blott, S.J.; Pye, K. Gradistat: A Grain Size Distribution and Statistics Package for the Analysis of Unconsolidated Sediments. *Earth Surf. Proc. Landforms* **2001**, *26*, 1237–1248. [CrossRef]
69. Walden, J. Sample collection and preparation. In *Environmental Magnetism: A Practical Guide*; Walden, J., Oldfield, F., Smith, J., Eds.; Quaternary Research Association: London, UK, 1999; pp. 63–88.
70. Maher, B.A. Magnetic properties of some synthetic sub-micronmagnetites. *Geophys. J.* **1988**, *94*, 83–96. [CrossRef]
71. Evans, M.E.; Heller, F. *Environmental Magnetism: Principles and Applications of Enviromagnetics*; Academic Press: San Diego, CA, USA, 2003; 299p.
72. Basavaiah, N. *Geomagnetism: Solid Earth and Upper Atmosphere Perspectives*; Springer: Dordrecht, The Netherlands, 2011. [CrossRef]
73. Basavaiah, N.; Khadkikar, S. Environmental Magnetism and its application towards paleomonsoon reconstruction. *J. Indian Geophys. Union* **2004**, *8*, 1–14.
74. Ghosh, R.; Saikia, K.; Biswas, O.; Agrawal, S.; Morthekai, P.; Arif, M.; Phartiyal, B.; Sharma, A.; Singh, N.; Paruya, D.K.; et al. Last 10 millennial history of Indian summer monsoon in the Bengal region–a multi-proxy reconstruction from a lacustrine archive. *Palaeogeogr. Palaeoclimatol. Palaeoecol.* **2023**, *609*, 111308. [CrossRef]
75. Dearing, J.A. Holocene environmental change from magnetic proxies in lake sediments. In *Quaternary Climates, Environments and Magnetism*; Maher, B.A., Thompson, R., Eds.; Cambridge University Press: Cambridge, UK, 1999; pp. 231–278.
76. Oldfield, F. Environmental magnetism—A personal perspective. *Quat. Sci. Rev.* **1991**, *10*, 73–85. [CrossRef]
77. Roberts, A.P.; Zhao, X.; Heslop, D.; Abrajevitch, A.; Chen, Y.H.; Hu, P.; Jiang, Z.; Liu, Q.; Pillans, B.J. Hematite (α-Fe_2O_3) quantification in sedimentary magnetism: Limitations of existing proxies and ways forward. *Geosci. Lett.* **2020**, *7*, 8. [CrossRef]
78. Sandeep, K.; Shankar, R.; Warrier, A.K.; Yadava, M.G.; Ramesh, R.; Jani, R.A.; Xuefeng, L. A multi-proxy lake sediment record of Indian summer monsoon variability during the Holocene in southern India. *Palaeogeogr. Palaeoclimatol. Palaeoecol.* **2017**, *476*, 1–14. [CrossRef]
79. Firbas, F. Der pollen analytische Nachweis des Getreidebaus. *Zeitschr. F. Bot.* **1937**, *31*, 447–478.
80. Hafstein, U. Pollen analytic investigations on the late-Quaternary development in the inner Oslofjord area. *Bergen Mus. Arb. Natury. K.* **1956**, *8*, 1–160.
81. Guinet, P. What may afford palynology to archaeology and ancient history in India? *JMS Univ. Baroda* **1966**, *15*, 15–19.
82. Bonnefille, R. Analyse pollinique d'un sediment recent: Vases actuelles de la riviereAouache (Ethiopie). *Pollen Spores* **1969**, *11*, 9–16.
83. Bhattacharyya, K.; Chanda, S. Late Quaternary vegetational history, palaeoecology and biostratigraphy of some deposits of Brahmaputra Basin, Upper Assam, India. *J. Palynol.* **1987**, *23–24*, 225–237.
84. Mazier, A.; Gallop, D.; Brun, C.; Butler, A. Modern pollen assemblage from grazed vegetation in the western Pyrenees, France: A numerical tool for more precise reconstruction of past cultural landscapes. *Holocene* **2006**, *16*, 91–103. [CrossRef]
85. Duane, D.B. Significance of skewness in recent sediments, western Pamlico Sound, North Carolina. *J. Sediment Petrol.* **1964**, *34*, 864–874.
86. Friedman, G.M. Dynamic processes and statistical parameters compared for size frequency distribution of beach and river sands. *J. Sediment. Petrol.* **1967**, *37*, 327–354.
87. Stanley-Wood, N.G.; Lines, R.W. *Particle Size Analysis*; Royal Society of Chemistry: London, UK, 2007.
88. Kanhaiya, S.; Singh, B.P. Spatial variation of textural parameters in a small river: An example from Khurar River, Khajuraho, Chhaterpur District, Madhya Pradesh, India. *Glob. J. Earth Sci. Eng.* **2014**, *1*, 34–42. [CrossRef]
89. Folk, R.L.; Ward, W.C. Brazos River bar: A study in the significance of grain size parameters. *J. Sediment. Petrol.* **1957**, *27*, 3–26. [CrossRef]
90. Folk, R.L. A review of grain size parameters. *Sedimentology* **1966**, *6*, 73–94. [CrossRef]
91. Snowball, I.F. Bacterial magnetite and the magnetic properties of sediments in a Swedish lake. *Earth Planet. Sci. Lett.* **1994**, *126*, 129–142. [CrossRef]
92. Snowball, I.F. Magnetic hysteresis properties of greigite (Fe_3S_4) and a new occurrence in Holocene sediments from Swedish Lappland. *Phys. Earth Planet. Inter.* **1991**, *68*, 32–40. [CrossRef]
93. Gautam, P.; Blaha, U.; Appel, E.; Neupane, G. Environmental magnetic approach towards the quantification of pollution in Kathmandu urban area, Nepal. *Phys. Chem. Earth* **2004**, *29*, 973–984. [CrossRef]
94. Anderson, N.J.; Rippey, B. Diagenesis of magnetic minerals in the recent sediments of a eutrophic lake. *Limnol. Oceanogr.* **1988**, *33*, 1476–1492. [CrossRef]
95. Bradley, R.S. *Palaeoclimatology: Reconstructing Climate of the Quaternary*; Academic Press Ltd.: London, UK, 1999.
96. Clement, S.; Prell, W.; Murry, D.; Shimmield, G.; Weedon, G. Forcing mechanisms of the Indian Ocean monsoon. *Nature* **1991**, *353*, 720–725. [CrossRef]
97. Xiao, J.L.; An, Z.S.; Liu, T.S.; Inouchi, Y.; Kumai, H.; Yoshikawa, S.; Kondo, Y. East Asian monsoon variation during the last 130,000 years: Evidence from the Loess Plateau of central China and Lake Biwa of Japan. *Quat. Sci. Rev.* **1999**, *18*, 147–157. [CrossRef]

98. Leuschner, D.C.; Sirocko, F. The low-latitude monsoon climate during Dansgaard-Oeschger cycles and Heinrich Events. *Quat. Sci. Rev.* **2000**, *19*, 243–254. [CrossRef]
99. Leuschner, D.C.; Sirocko, F. Orbital insolation forcing of the Indian monsoon ea motor for global climate change? *Palaeogeogr. Palaeoclimatol. Palaeoecol.* **2003**, *197*, 83–95. [CrossRef]
100. Altabet, M.A.; Higginson, M.J.; Murray, D.W. The effect of millennial-scale changes in Arabian Sea de-nitrification on atmospheric CO_2. *Nature* **2002**, *415*, 159–162. [CrossRef]
101. Loulergue, L.; Schilt, A.; Spahni, R.; Masson-Delmotte, V.; Blunier, T.; Lemieux, B.; Barnola, J.M.; Raynaud, D.; Stocker, T.F.; Chappellaz, J. Orbital and millennial-scale features of atmospheric CH_4 over the past 800,000 years. *Nature* **2008**, *453*, 383–386. [CrossRef]
102. Wang, Y.J.; Cheng, H.; Edwards, R.L.; Kong, X.; Shao, X.; Chen, S.; Wu, J.; Jiang, X.; Wang, X.; An, Z. Millennial- and orbital-scale changes in the east Asian monsoon over the past 224,000 years. *Nature* **2008**, *451*, 1090–1093. [CrossRef]
103. Duplessy, J.C. Glacial to interglacial contrasts in the northern Indian Ocean. *Nature* **1982**, *295*, 494–498. [CrossRef]
104. Rahaman, R.; Singh, S.K.; Sinha, R.; Tandon, S.K. Climate control on erosion distribution over the Himalaya during the past ~100 ka. *Geology* **2009**, *37*, 559–562. [CrossRef]
105. Agrawal, S.; Sanyal, P.; Sarkar, A.; Jaiswal, M.J.; Dutta, K. Variability of Indian monsoonal rainfall over the past 100 ka and its implication for C3-C4 vegetational change. *Quat. Res.* **2012**, *77*, 159–170. [CrossRef]
106. Agrawal, S.; Galy, V.; Sanyal, P.; Eglinton, T. C4 plant expansion in the Ganga Plain during the last glacial cycle:Insights from isotopic composition of vascular plant biomarkers. *Org. Geochem.* **2014**, *67*, 58–71. [CrossRef]
107. Trivedi, A.; Saxena, A.; Chauhan, M.; Sharma, A.; Farooqui, A.; Nautiyal, C.; Yao, Y.-F.; Wang, Y.-F.; Li, C.-S.; Tiwari, D. Vegetation, climate and culture in Central Ganga plain, India: A multi-proxy record for Last Glacial Maximum. *Quat. Int.* **2019**, *507*, 137–147. [CrossRef]
108. Patnaik, R.; Chauhan, P.R.; Rao, M.R.; Blackwell, B.A.B.; Skinner, A.R.; Sahni, A.; Khan, H.S. New geochronological, paleoclimatological, and archaeological data from the Narmada Valley hominin locality, central India. *J. Human Evol.* **2009**, *56*, 114–133. [CrossRef]
109. Sukumar, R.; Ramesh, R.; Pant, R.K.; Rajagopalan, G. A δ13C record of late Quaternary climate change from tropical peats in southern India. *Nature* **1993**, *364*, 703–706. [CrossRef]
110. Sharma, C.; Chauhan, M.S. Vegetation and climate since last glacial maximum in Darjeeling (Mirik Lake), Eastern Himalaya. In *Proceedings of the 29th International Geological Congress Part B*; CRC Press: Boca Raton, FL, USA, 1994; pp. 279–288.
111. Wasson, R.J.; Smith, G.I.; Agrawal, D.P. Late quaternary sediments, minerals and inferred geochemical history of DidwanaLake, TharDesert, India. *Palaeogeogr. Palaeoclimatol. Palaeoecol.* **1984**, *46*, 345–372. [CrossRef]
112. Huguet, C.; Routh, J.; Feitz, S.; Lone, M.A.; Kalpana, M.S.; Ghosh, P.; Mangini, A.; Kumar, V.; Rangarajan, A. Temperature and monsoon tango in a tropical stalagmite: Last glacial-interglacial climate dynamics. *Sci. Rep.* **2018**, *8*, 5386. [CrossRef]
113. Bhattacharyya, A.; Mehrotra, N.; Shah, S.K.; Basavaiah, N.; Chaudhary, V.; Singh, I.B. Analysis of vegetation and climate change during late Pleistocene from Ziro Valley, Arunachal Pradesh, Eastern Himalaya region. *Quat. Sci. Rev.* **2014**, *101*, 111–123. [CrossRef]
114. Ghosh, R.; Bera, S.; Sarkar, A.; Paruya, D.K.; Yao, Y.-F.; Li, C.-S. A ~50 ka record of monsoonal variability in the Darjeeling foothill region, eastern Himalayas. *Quat. Sci. Rev.* **2015**, *114*, 100–115. [CrossRef]
115. Kotlia, B.S.; Sanwal, J.; Phartiyal, B.; Joshi, L.M.; Trivedi, A.; Sharma, C. Late Quaternary climatic changes in the eastern Kumaun Himalaya, India, as deduced from multi-proxy studies. *Quat. Int.* **2010**, *213*, 44–55. [CrossRef]
116. Premathilake, R.; Risberg, J. Late Quaternary climate history from the Horton Plains, central Sri Lanka. *Quat. Sci. Rev.* **2003**, *22*, 1525–1541. [CrossRef]
117. Premathilake, R. Late Pleistocene and Early Holocene Climate and Environmental Changes in the Horton Plains, Central Sri Lanka. *Quat. Sci. Rev.* **2012**, *50*, 23–42. [CrossRef]
118. Zhang, E.; Sun, W.; Chang, J.; Ning, D.; Shulmeister, J. Variations in the Indian summer monsoon over the last 30,000 years inferred from a pyrogenic carbon record from south-west China. *J. Quat. Sci.* **2018**, *33*, 131–138. [CrossRef]
119. Yu, G.; Xue, B.; Wang, S.; Liu, J. Lake records and LGM climate in China. *Chin. Sci. Bull.* **2000**, *45*, 1158–1164. [CrossRef]
120. Agnihotri, R.; Sarin, M.M.; Somayajulu, B.L.K.; Jull, A.J.T.; Burr, G.S. Late-Quaternary biogenic productivity and organic carbon deposition in the eastern Arabian Sea. *Palaeogeogr. Palaeoclimatol. Palaeoecol.* **2003**, *197*, 43–60. [CrossRef]
121. Nambiar, R.; Bhushan, R.; Raj, H. Paleoredox conditions of bottom water in the northern Indian Ocean since 39 ka. *Palaeogeogr. Palaeoclimatol. Palaeoecol.* **2022**, *586*, 110766. [CrossRef]
122. Neelavannan, K.; Hussain, S.M.; Nishath, N.M.; Achyuthan, H.; Veerasingam, S.; Prakasam, M.; Kumar, P.; Singh, P.; Kurian, P.J. Paleoproductivity shifts since the last 130 ka off Lakshadweep, Southeastern Arabian Sea. *Reg. Stud. Mar. Sci.* **2021**, *44*, 101776. [CrossRef]
123. Anand, P.; Kroon, D.; Singh, A.D.; Ganeshram, R.S.; Ganssen, G.; Elderfield, H. Coupled sea surface temperature-seawater $\delta^{18}O$ reconstructions in the Arabian Sea at the millennial scale for the last 35 ka. *Paleoceanography* **2008**, *23*, 1–8. [CrossRef]
124. Clemens, S.C.; Yamamoto, M.; Thirumalai, K.; Giosan, L.; Richey, J.N.; Nilsson-Kerr, K.; Rosenthal, Y.; Anand, P.; McGrath, S.M. Remote and local drivers of pleistocene south asian summer monsoon precipitation: A test for future predictions. *Sci. Adv.* **2021**, *7*, eabg3848. [CrossRef]

125. Govil, P.; Naidu, P.D. Variations of indian monsoon precipitation during the last 32kyr reflected in the surface hydrography of the Western Bay of Bengal. *Quat. Sci. Rev.* **2011**, *30*, 3871–3879. [CrossRef]
126. Ahmad, S.M.; Zheng, H.; Raza, W.; Zhou, B.; Lone, M.A.; Raza, T.; Suseela, G. Glacial to Holocene changes in the surface and deep waters of the Northeast Indian Ocean. *Mar. Geol.* **2012**, *329–331*, 16–23. [CrossRef]
127. Kudrass, H.; Hofmann, A.; Doose, H.; Emeis, K.; Erlenkeuser, H. Modulation and amplification of climatic changes in the Northern Hemisphere by the Indian summer monsoon during the past 80 k.y. *Geology* **2001**, *29*, 63–66. [CrossRef]
128. Raza, T.; Ahmad, S.M.; Sahoo, M.; Banerjee, B.; Bal, I.; Dash, S.; Suseela, G.; Mukherjee, I. Hydrographic changes in the southern Bay of Bengal during the last ~65,000 yr inferred from carbon and oxygen isotopes of foraminiferal fossil shells. *Quat. Int.* **2014**, *333*, 77–85. [CrossRef]
129. Rashid, H.; England, E.; Thompson, L.; Polyak, L. Late glacial to Holocene Indian Summer Monsoon variability based upon sediment records taken from the Bay of Bengal. *Terr. Atmos. Ocean. Sci.* **2011**, *22*, 215–228. [CrossRef]
130. Liu, S.; Li, J.; Zhang, H.; Cao, P.; Mi, B.; Khokiattiwong, S.; Kornkanitnan, N.; Shi, X. Complex response of weathering intensity registered in the Andaman Sea sediments to the Indian Summer Monsoon over the last 40 kyr. *Mar. Geol.* **2020**, *426*, 106206. [CrossRef]
131. Phillips, S.C.; Johnson, J.E.; Giosan, L.; Rose, K. Monsoon-influenced variation in productivity and lithogenic sediment flux since 110ka in the offshore Mahanadi Basin, northern Bay of Bengal. *Mar. Pet. Geol.* **2014**, *58*, 502–525. [CrossRef]
132. Panmei, C.; Naidu, P.D.; Naik, S.S. Variability of terrigenous input to the Bay of Bengal for the last ~80 kyr: Implications on the Indian monsoon variability. *Geo Mar. Lett.* **2018**, *38*, 341–350. [CrossRef]
133. Wu, G.; Yao, T.; Thompson, L.G.; Li, Z. Microparticle record in the Guliya ice core and its comparison with polar records since the last interglacial. *Chin. Sci. Bull.* **2004**, *49*, 607–611. [CrossRef]
134. Mahowald, N.; Kohfeld, K.; Hansson, M.; Balkanski, Y.; Harrison, S.P.; Prentice, I.C.; Schulz, M.; Rodhe, H. Dust sources and deposition during the Last Glacial Maximum and current climate: A comparison of model results with paleodata from ice cores and marine sediments. *J. Geophys. Res. Atmos.* **1999**, *104*, 15895–15916. [CrossRef]
135. Benarde, M.A. *Global Warming*; John Wiley and Sons: New York, NY, USA, 1992.
136. Banerji, U.S.; Arulbalaji, P.; Padmalal, D. Holocene climate variability and Indian Summer Monsoon: An overview. *Holocene* **2020**, *30*, 744–773. [CrossRef]
137. Banerji, U.S.; Padmalal, D.; Sciences, E. Bond events and monsoon variability during Holocene-Evidence from marine and continental archives. In *Holocene Climate Change and Environment*; Kumaran, K.P.N., Padmalal, D., Eds.; Elsevier: Amsterdam, The Netherlands, 2022; pp. 293–338. [CrossRef]
138. Haug, G.H.; Hughen, K.A.; Sigman, D.M.; Peterson, L.C.; Rohl, U. Southward migration of the intertropical convergence zone through the Holocene. *Science* **2001**, *293*, 1304–1308. [CrossRef] [PubMed]
139. Gupta, P.; Gupta, A.K.; Clemens, S.C.; Cheng, H.; Majhi, B. Coupled Ocean-atmospheric forcing on Indian Summer Monsoon variability during the middle Holocene: Insights from the Core Monsoon Zone speleothem record. *Palaeogeogr. Palaeoclimatol. Palaeoecol.* **2024**, *647*, 112273. [CrossRef]
140. Berger, A.; Loutre, M.F.; Mélice, J.L. Equatorial insolation: From precession harmonics to eccentricity frequencies. *Clim. Past* **2006**, *2*, 131–136. [CrossRef]
141. Agnihotri, R.; Dutta, K.; Bhushan, R.; Somayajulu, B.L.K. Evidence for solar forcing on the Indian monsoon during the last millennium. *Earth Planet. Sci. Lett.* **2002**, *198*, 521–527. [CrossRef]
142. Band, S.; Yadava, M.; Lone, M.A.; Shen, C.-C.; Sree, K.; Ramesh, R. High-resolutionmid-Holocene Indian SummerMonsoon recorded in a stalagmite from the Kotumsar Cave, Central India. *Quat. Int.* **2018**, *479*, 19–24. [CrossRef]
143. Sharma, S.; Joachimski, M.; Sharma, M.; Tobschall, H.J.; Singh, I.B.; Sharma, C.; Chauhan, M.S.; Morgeroth, G. Late Glacial and Holocene environmental changes in Ganga Plain, Northern India. *Quat. Sci. Rev.* **2004**, *23*, 45–159. [CrossRef]
144. Williams, M.A.J.; Clarke, M.F. Late Quaternary environments in North-Central India. *Nature* **1984**, *308*, 633–635. [CrossRef]
145. Singh, G.; Joshi, R.D.; Singh, A.B. Stratigraphic and radiocarbon evidence for the age and development of three salt lake deposits in Rajasthan, India. *Quat. Res.* **1972**, *2*, 496–505. [CrossRef]
146. Singh, G.; Joshi, R.D.; Chopra, S.K.; Singh, A.B. Late Quaternary history of vegetation and climate of the Rajasthan Desert, India. *Phil. Trans. R. Soc. Lond.* **1974**, *267*, 467–501.
147. Bryson, R.A.; Swain, A.M. Holocene variations of monsoon rainfall in Rajasthan. *Quat. Res.* **1981**, *16*, 135–145. [CrossRef]
148. Swain, A.M.; Kutzbach, J.E.; Hastenrath, S. Estimates of Holocene precipitation for Rajasthan, India, based on pollen and lake-level data. *Quat. Res.* **1983**, *19*, 1–17. [CrossRef]
149. Kaufman, D.S.; Ager, T.A.; Anderson, N.J.; Anderson, P.M.; Andrews, J.T.; Bartlein, P.J.; Brubaker, L.B.; Coats, L.L.; Cwynar, L.C.; Duvall, M.L.; et al. Holocene thermal maximum in the western Arctic (0–180° W). *Quat. Sci. Rev.* **2004**, *23*, 529–560. [CrossRef]
150. Jansen, E.; Overpeck, J.T.; Briffa, K.R.; Duplessy, J.C.; Joos, F.; Masson-Delmotte, V.; Olago, D.; Otto-Bliesner, B.; Peltier, W.R.; Rahmstorf, S.; et al. Palaeoclimate. In *Climate Change: The Physical Science Basis*; Solomon, S., Qin, D., Manning, M., Chen, Z., Marquis, M., Averyt, K.B., Tignor, M., Miller, H.L., Eds.; 4th Assessment Report IPCC; Cambridge Univ. Press: Cambridge, UK, 2007; pp. 433–498.
151. Jansen, E.; Andersson, C.; Moros, M.; Nisancioglu, K.H.; Nyland, B.F.; Telford, R.J. The early to mid-Holocene thermal optimum in the North Atlantic. In *Natural Climate Variability and Global Warming: A Holocene Perspective*; Battarbee, R.W., Binney, H.A., Eds.; Wiley-Blackwell: Chichester, UK, 2008; pp. 123–137.

152. Wanner, H.; Beer, J.; Butikofer, J.; Crowley, T.J.; Cubasch, U.; Fluckiger, J.; Goosse, H.; Grosjean, M.; Joos, F.; Kaplan, J.O.; et al. Mid-to Late Holocene climate change: An overview. *Quat. Sci. Rev.* **2008**, *27*, 1791–1828. [CrossRef]
153. Miller, G.; Brigham-Grette, J.; Alley, R.; Anderson, L.; Bauch, H.; Douglas, M.; Edwards, M.; Elias, S.; Finney, B.; Fitzpatrick, J.; et al. Temperature and precipitation history of the Arctic. *Quat. Sci. Rev.* **2010**, *29*, 1679–1715. [CrossRef]
154. Bartlein, P.J.; Harrison, S.P.; Brewer, S.; Connor, S.; Davis, B.A.S.; Gajewski, K.; Guiot, J.; Harrison-Prentice, T.I.; Henderson, A.; Peyron, O.; et al. Pollen-based continental climate reconstructions at 6 and 21 ka: A global synthesis. *Clim. Dyn.* **2011**, *37*, 755–802. [CrossRef]
155. Renssen, H.; Seppä, H.; Crosta, X.; Goosse, H.; Roche, D.M. Global characterization of the Holocene Thermal Maximum. *Quat. Sci. Rev.* **2012**, *48*, 7–19. [CrossRef]
156. Quamar, M.F.; Singh, A.K.; Joshi, L.M.; Kotlia, B.S.; Singh, D.S.; Simion, C.A.; Sava, T.; Prasad, N. Vegetation dynamics and hydro-climatic changes during the Middle Holocene from the Central Himalaya, India. *Quaternary* **2023**, *6*, 11. [CrossRef]
157. Quamar, M.F.; Banerji, U.S.; Thakur, B.; Kar, R. Hydroclimatic changes in the Core Monsoon Zone of India since the Last Glacial Maximum: An overview of the palynological data and correlation with the marine and continental records. *Palaeogeogr. Palaeoclimatol. Palaeoecol.* **2024**, *633*, 111844. [CrossRef]